# CHAPTER 5

# ANALYSIS OF WAVESHAPE AND WAVEFORM COMPLEXITY

Certain biomedical signals, such as the ECG and the carotid pulse, have simple waveshapes (although the QRS wave is often referred to as a *complex*!). The readily identifiable signatures of the ECG and the carotid pulse are modified by abnormal events and pathological processes. Hence, analysis of waveshapes could be useful in the diagnosis of various diseases.

Signals such as the EMG and the PCG do not have waveshapes that may be identified easily. EMG signals are complex interference patterns of innumerable SMUAPs. PCG signals represent vibration waves that do not possess specific waveshapes. Regardless, even the complexity of the waveforms in some signals, such as the EMG and the PCG, does vary in relation to physiological and pathological phenomena. Analyzing the waveform complexity of such signals may assist in gaining an understanding of the processes they reflect.

*Biomedical Signal Analysis, Second Edition. By Rangaraj M. Rangayyan*

## 5.1 Problem Statement

*Explain how waveshapes and waveform complexity in biomedical signals relate to the characteristics of the underlying physiological and pathological phenomena. Propose techniques to parameterize and analyze the signal features you identify.*

As in the preceding chapters, the problem statement given above is generic and represents the theme of the present chapter. The following section presents illustrations of the problem with case studies that provide more specific definitions of the problem with a few signals of interest. The remaining sections of the chapter describe techniques to address the stated problems. It should be noted that, although signal analysis techniques are proposed in the context of specific signals and applications, they may find applications in other fields where signals with comparable characteristics and behavior are encountered.

## 5.2 Illustration of the Problem with Case Studies

### 5.2.1 The QRS complex in the case of bundle branch block

We saw in Section 1.2.5 that the His bundle and its branches conduct the cardiac excitation pulse from the AV node to the ventricles. A block in one of the bundle branches causes asynchrony between the contraction of the left and the right ventricles. This, in turn, causes a staggered summation of the action potentials of the myocytes of the left and the right ventricles over a longer-than-normal duration. The result is a longer and possibly jagged QRS complex, as illustrated by the ECG of a patient with right bundle-branch block in Figure 1.28.

### 5.2.2 The effect of myocardial ischemia and infarction on QRS wave shape

The occlusion of a coronary artery, or a branch thereof, due to the deposition of fat, calcium, and other substances, results in reduced blood supply to a portion of the cardiac musculature. The part of the myocardium served by the affected artery then suffers from ischemia, that is, lack of blood supply. Complete blockage of an artery leads to myocardial infarction when the affected tissues die. The deceased myocytes cannot contract any more and no longer produce action potentials.

The action potential of an under-nourished ventricular myocyte reflects altered repolarization characteristics: The action potential is of smaller amplitude and shorter duration [11, 233] than the normal case. The result of the summation of the action potentials of all of the active ventricular myocytes will then be different from the normal QRS complex. The primary change reflected in the ECG is a modified ST segment that is either elevated or depressed, depending upon the lead used and the position of the affected region; the T wave may also be inverted. Chronic myocardial infarction causes a return to a normal ST segment and a pronounced Q wave [33].

### 5.2.3 Ectopic beats

Ectopic beats are generated by cardiac tissues that possess abnormal pacing capabilities. Ectopic beats originating from focal points on the atria could cause altered P waveshapes due to different paths of propagation of the excitation pulse and hence different activation sequences of atrial muscle fibers. However, the QRS complex of atrial ectopic beats will appear normal because the conduction of the excitation past the AV node would be normal.

Ectopic beats originating on the ventricles (that are necessarily premature beats, that is, PVCs) typically possess bizarre waveshapes due to widely differing paths of conduction and excitation of the ventricular muscle fibers. Figure 1.27 illustrates an ECG signal with PVCs. PVCs typically lack a preceding P wave; however, an ectopic beat triggered during the normal AV node delay will demonstrate a normal preceding P wave. PVCs triggered by ectopic foci close to the AV node may possess near-normal QRS shape as the path of conduction may be almost the same as in the case of a normal impulse from the AV node. On the other hand, beats triggered by ectopic foci near the apex of the heart could take widely different paths of propagation, resulting in substantially different QRS waveshapes. In addition to waveshape, the preceding and succeeding $RR$ intervals play important roles in determining the nature of ectopic beats.

### 5.2.4 Complexity of the EMG interference pattern

We saw in Section 1.2.4 that motor units are recruited by two mechanisms — spatial and temporal recruitment — in order to produce increasing levels of contraction and muscular force output. As more and more motor units are brought into action and their individual firing rates increase (within certain limits), the SMUAPs of the active motor units overlap and produce a complex interference pattern. Figures 1.18 and 1.19 illustrate an EMG signal obtained from the crural diaphragm of a dog during one normal breath cycle. The increasing complexity of the waveform with deeper levels of inspiration is clearly seen in the expanded plot in Figure 1.19.

Although a surface EMG interference pattern is typically too complex for visual analysis, the general increase in the level of activity ("busy-ness") may be readily seen. It used to be common practice in EMG laboratories to feed EMG signals to an amplified speaker: low levels of activity when the SMUAPs are not overlapping (that is, separated in time) result in discrete "firing" type of sounds; increasing levels of contraction result in increased "chatter" in the sound produced. EMG signals may be analyzed to derive parameters of waveform complexity that increase with increasing muscular contraction, and hence to obtain correlates to mechanical activity that are derived from its electrical manifestation.

### 5.2.5 PCG intensity patterns

Although the vibration waves in a PCG signal may not be amenable to direct visual analysis, the general intensity pattern of the signal over a cardiac cycle may be

readily appreciated either by auscultation or visual inspection. Certain cardiovascular diseases and defects alter the relative intensity patterns of S1 and S2, cause additional sounds or murmurs, and/or split S2 into two distinct components, as described in Section 1.2.9. While many cardiovascular diseases and defects may cause systolic murmurs, the intensity pattern or envelope of the murmur could assist in arriving at a specific diagnosis. It should also be noted that definitive diagnosis based on the PCG would usually require comparative analysis of PCG signals from a few positions on the chest. Figures 1.42, 1.44, 4.30, and 4.31 illustrate PCG signals of a normal subject and patients with systolic murmur, split S2, and opening snap of the mitral valve. The differences in the overall intensity patterns of the signals are obvious. However, signal processing techniques are desirable to convert the signals into positive-valued envelopes that could be treated as distributions of signal energy over time. Such a transformation permits the treatment of signal intensity patterns as PDFs, which lends to the computation of various statistical measures and moments.

## 5.3 Analysis of ERPs

The most important parameter extracted from a visual ERP is the timing or latency of the first major positivity; since the average of this latency is about $120\ ms$ for normal adults, it is referred to as P120 (see Figure 3.41). The latencies of the troughs before and after P120, called N80 and N145, respectively, are also of interest. The amplitudes of the ERP at the corresponding instants are of lesser importance. Delays in the latencies that are well beyond the normal range could indicate problems in the visual system. Asymmetries in the latencies of the left and right parts of the visual system could also be indicative of disorders.

The lowest trace in Figure 3.41 is an averaged flash visual ERP recorded from a normal adult male subject. The signal has been labeled to indicate the N80, P120, and N145 points; the corresponding actual latencies for the subject are $85, 100.7,$ and $117\ ms$, respectively.

Auditory ERPs are weaker and more complex than visual ERPs, requiring averaging over several hundred or a few thousand stimuli. Auditory ERPs are analyzed for the latencies and amplitudes of several peaks and troughs. Clinical ERP analysis is usually performed manually, since there is no pressing need for signal processing techniques beyond synchronized averaging.

## 5.4 Morphological Analysis of ECG Waves

The waveshape of an ECG cycle could be changed by many different abnormalities, including myocardial ischemia or infarction, bundle-branch block, and ectopic beats. It is not possible to propose a single analysis technique that can assist in categorizing all possible abnormal causes of change in waveshape. The following sections address a few illustrative cases.

### 5.4.1 Correlation coefficient

**Problem:** *Propose a general index to indicate altered QRS waveshape. You are given a normal QRS template.*

**Solution:** Jenkins et al. [132] applied the correlation coefficient $\gamma_{xy}$ as defined in Equation 4.24 to classify ECG cycles as normal beats or beats with abnormal morphology. A normal beat was used as a template to compute $\gamma_{xy}$ for each detected beat. They found that most normal beats possessed $\gamma_{xy}$ values above $0.9$, and that PVCs and beats with abnormal shape had considerably lower values. A threshold of $0.9$ was used to assign a code to each beat as $0$ for abnormal or $1$ for normal in terms of waveshape. Figure 2.2 shows an ECG signal with five abnormal beats that have the first symbol in the $4$-symbol code shown for each beat as $0$, indicating an abnormal shape due to generation by an ectopic focus or due to aberrant conduction of a pulse generated by the SA node. The normal beats have the first symbol of the code as $1$, indicating high correlation with the normal template. See Section 5.8 for related discussion.

### 5.4.2 The minimum phase correspondent and signal length

The normal ECG signal contains epochs of activity where the signal's energy is concentrated. Discounting the usually low-amplitude P and T waves, most of the energy of a normal ECG signal is concentrated within the interval of about $80\ ms$ that is spanned by the QRS complex. The normally isoelectric PQ, ST, and TP segments contain no energy as the signal amplitude is typically zero over the corresponding intervals. We have observed that certain abnormal conditions cause the QRS to widen or the ST segment to possess a nonzero value. In such a case, it could be said that the energy of the signal is being spread over a longer duration. Let us now consider how we may capture this information, and investigate if it may be used for waveshape analysis.

**Problem:** *Investigate the effect of the distribution of energy over the time axis on a signal's characteristics. Propose measures to parameterize the effects and study their use in the classification of ECG beats.*

**Solution:** A signal $x(t)$ may be seen as a distribution of the amplitude of a certain variable over the time axis. The square of the signal, that is, $x^2(t)$, may be interpreted as the instantaneous energy of the signal-generating process. The function $x^2(t),\ 0 \leq t \leq T$, may then be viewed as an energy distribution or density function, with the observation that the total energy of the signal is given by

$$E_x = \int_0^T x^2(t)\, dt. \tag{5.1}$$

Such a representation facilitates the definition of moments of the energy distribution, leading to a centroidal time

$$t_{\bar{x}} = \frac{\int_0^T t\ x^2(t)\, dt}{\int_0^T x^2(t)\, dt}, \tag{5.2}$$

and dispersion of energy about the centroidal time

$$\sigma^2_{t_{\bar{x}}} = \frac{\int_0^T (t - t_{\bar{x}})^2 \, x^2(t) \, dt}{\int_0^T x^2(t) \, dt}. \tag{5.3}$$

Observe the similarity between the equations given above and Equations 3.1 and 3.3: The normalized function

$$p_x(t) = \frac{x^2(t)}{\int_0^T x^2(t) \, dt} \tag{5.4}$$

is now treated as a PDF. Other moments may also be defined to characterize and study the distribution of $x^2(t)$ over the time axis. The preceding equations have been stated in continuous time for the sake of generality; they are valid for discrete-time signals, with a simple change of $t$ to $n$ and $\int \, dt$ to $\sum_n$.

**Minimum-phase signals:** The distribution of the energy of a signal over its duration is related to its amplitude spectrum and, more importantly, to its phase spectrum. The notion of minimum phase is useful in analyzing related signal characteristics. The minimum-phase property of signals may be explained in both the time and frequency domains [174, 201, 234–238].

In the time domain, a signal $x(n)$ is a minimum-phase signal if both the signal and its inverse $x_i(n)$ are one-sided (that is, completely causal or anticausal) signals with finite energy, that is, $\sum_{n=0}^{\infty} x^2(n) < \infty$ and $\sum_{n=0}^{\infty} x_i^2(n) < \infty$. [*Note:* The inverse of a signal is defined such that $x(n) * x_i(n) = \delta(n)$; equivalently, we have $X_i(z) = \frac{1}{X(z)}$.]

Some of the important properties of a minimum-phase signal are:

- For a given amplitude spectrum there exists one and only one minimum-phase signal.
- Of all finite-energy, one-sided signals with identical amplitude spectra, the energy of the minimum-phase signal is optimally concentrated toward the origin, and the signal has the smallest phase lag and phase-lag derivative at each frequency.
- The $z$-transform of a minimum-phase signal has all of its poles and zeros inside the unit circle in the $z$-plane.
- The complex cepstrum of a minimum-phase signal is causal (see also Section 4.8.3).

The extreme example of a minimum-phase signal is the delta function $\delta(t)$, which has all of its energy concentrated at $t = 0$. The magnitude spectrum of the delta function is real and equal to unity for all frequencies; the phase lag at every frequency is zero.

**Minimum-phase and maximum-phase components:** A signal $x(n)$ that does not satisfy the minimum-phase condition, referred to as a composite signal or a

mixed-phase signal, may be split into its minimum-phase component and maximum-phase component by filtering its complex cepstrum $\hat{x}(n)$ [174, 223, 239]. To obtain the minimum-phase component, the causal part of the complex cepstrum (see Section 4.8.3) is chosen as follows:

$$\hat{x}_{\min}(n) = \begin{cases} 0, & n < 0, \\ 0.5\,\hat{x}(n), & n = 0, \\ \hat{x}(n), & n > 0. \end{cases} \tag{5.5}$$

Application of the inverse procedures yields the minimum-phase component $x_{\min}(n)$. Similarly, the maximum-phase component is obtained by application of the inverse procedures to the anticausal part of the cepstrum, selected as

$$\hat{x}_{\max}(n) = \begin{cases} \hat{x}(n), & n < 0, \\ 0.5\,\hat{x}(n), & n = 0, \\ 0, & n > 0. \end{cases} \tag{5.6}$$

The minimum-phase and maximum-phase components of a signal satisfy the following relationships:

$$\hat{x}(n) = \hat{x}_{\min}(n) + \hat{x}_{\max}(n) \tag{5.7}$$

and

$$x(n) = x_{\min}(n) * x_{\max}(n). \tag{5.8}$$

**The minimum-phase correspondent:** A mixed-phase signal may be converted to a minimum-phase signal that has the same spectral magnitude as the original signal by filtering the complex cepstrum of the original signal as

$$\hat{x}_{\mathrm{MPC}}(n) = \begin{cases} 0, & n < 0, \\ \hat{x}(n), & n = 0, \\ \hat{x}(n) + \hat{x}(-n), & n > 0, \end{cases} \tag{5.9}$$

and applying the inverse procedures [174, 223, 239]. The result is known as the *minimum-phase correspondent* (MPC) of the original signal [201]. The MPC possesses optimal concentration of energy near the origin under the constraint imposed by the specified magnitude spectrum (of the original mixed-phase signal).

Observe that $\hat{x}_{\mathrm{MPC}}(n)$ is equal to twice the even part of $\hat{x}(n)$ for $n > 0$. This leads to a simpler procedure to compute the MPC, as follows. Let us assume $\hat{X}(z) = \log X(z)$ to be analytic over the unit circle in the $z$-plane. We can write $\hat{X}(\omega) = \hat{X}_R(\omega) + j\hat{X}_I(\omega)$, where the subscripts $R$ and $I$ indicate the real and imaginary parts, respectively. $\hat{X}_R(\omega)$ and $\hat{X}_I(\omega)$ are the log-magnitude and phase spectra of $x(n)$, respectively. Now, the inverse Fourier transform of $\hat{X}_R(\omega)$ is equal to the even part of $\hat{x}(n)$, defined as $\hat{x}_e(n) = [\hat{x}(n) + \hat{x}(-n)]/2$. Thus, we have

$$\hat{x}_{\mathrm{MPC}}(n) = \begin{cases} 0, & n < 0, \\ \hat{x}_e(n), & n = 0, \\ 2\,\hat{x}_e(n), & n > 0. \end{cases} \tag{5.10}$$

This result means that we do not need to compute the complex cepstrum, which requires the unwrapped phase spectrum of the signal, but need only to compute a *real cepstrum* using the log-magnitude spectrum. Furthermore, given that the PSD is the Fourier transform of the ACF, we have $\log\{\mathrm{FT}[\phi_{xx}(n)]\} = 2\hat{X}_R(\omega)$. It follows that, in the cepstral domain, $\hat{\phi}_{xx}(n) = 2\hat{x}_e(n)$, and therefore [239]

$$\hat{x}_{\mathrm{MPC}}(n) = \begin{cases} 0, & n < 0, \\ 0.5\,\hat{\phi}_{xx}(n), & n = 0, \\ \hat{\phi}_{xx}(n), & n > 0, \end{cases} \tag{5.11}$$

where $\hat{\phi}_{xx}(n)$ is the cepstrum of the ACF $\phi_{xx}(n)$ of $x(n)$.

**Signal length:** The notion of signal length ($SL$), as introduced by Berkhout [235], is different from signal duration. The duration of a signal is the extent of time over which the signal exists, that is, has nonzero values (neglecting periods within the total duration of the signal where the signal's amplitude could be zero). $SL$ relates to how the energy of a signal is distributed over its duration. $SL$ depends upon both the magnitude and phase spectra of the signal. For one-sided signals, minimum $SL$ implies minimum phase; the converse is also true [235].

The general definition of the $SL$ of a signal $x(n)$ is given as [235]

$$SL = \frac{\sum_{n=0}^{N-1} w(n)\, x^2(n)}{\sum_{n=0}^{N-1} x^2(n)}, \tag{5.12}$$

where $w(n)$ is a nondecreasing, positive weighting function with $w(0) = 0$. The definition of $w(n)$ depends upon the application and the desired characteristics of $SL$. It is readily seen that samples of the signal away from the origin $n = 0$ receive progressively heavier weights given by $w(n)$. The definition of $SL$ as above may be viewed as a normalized moment of $x^2(n)$. If $w(n) = n$, we get the centroidal time instant of $x^2(n)$ as in Equation 5.2.

For a given amplitude spectrum and hence total energy, the minimum-phase signal has its energy optimally concentrated near the origin. Therefore, the minimum-phase signal will have the lowest $SL$ of all signals with the specified amplitude spectrum. Signals with increasing phase lag have their energy spread over a longer time duration and will have larger $SL$ due to the increased weighting by $w(n)$.

**Illustration of application:** The QRS-T wave is the result of the spatiotemporal summation of the action potentials of ventricular myocytes. The duration of normal QRS-T waves is in the range of $350 - 400\ ms$, with the QRS itself limited to about $80\ ms$ due to rapid and coordinated depolarization of the ventricular muscle fibers via the Purkinje fibers. However, PVCs, in general, have QRS-T complexes that are wider than normal, that is, they have their energy distributed over longer time spans within their total duration. This is due to different and possibly slower and disorganized excitation sequences triggering the ventricular muscle fibers: Ectopic triggers may not get conducted through the Purkinje system, and may be conducted through the ventricular muscle fibers themselves. Furthermore, PVCs do not, in general, display separate QRS and T waves; that is, they lack an isoelectric ST segment.

Regardless of the distinctions described above, normal ECG beats and PVCs have similar amplitude spectra, indicating that the difference between the signals may lie in their phase. $SL$ depends upon both the amplitude spectrum and the phase spectrum of the given signal, and it parameterizes the distribution of energy over the duration of the signal. Based upon the arguments above, Murthy and Rangaraj [201] proposed the application of $SL$ to classify ECG beats as normal or ectopic (or PVC, along with the use of the $RR$ interval to indicate prematurity). Furthermore, to overcome ambiguities in the determination of the onset of each beat, they computed the $SL$ of the MPC of the ECG signals (segmented so as to include the P, QRS, and T waves of each cycle). Use of the MPC resulted in a "rearrangement" of the signal such that the dominant QRS wave appeared at the origin in the MPC.

Figure 5.1 illustrates a normal ECG signal and three PVCs of a patient with multiple ectopic foci generating PVCs of widely differing shapes [201]. The figure also illustrates the corresponding MPCs and lists the $SL$ values of all of the signals. The $SL$ values of the MPCs of the abnormal waves are higher than the $SL$ of the MPC of the normal signal (see the right-hand column of signals in Figure 5.1). The $SL$ values of the original PVCs do not exhibit such a separation from the $SL$ of the normal signal (see the left-hand column of signals in Figure 5.1). Ambiguities due to the presence of baseline segments of variable lengths at the beginning of the signals have been overcome by the use of the MPCs. In each case, the MPCs have the most-dominant wave at the origin, reflecting a rearrangement of energy in order to meet the minimum-phase criteria.

Figure 5.2 shows plots of the $RR$ intervals and $SL$ values computed using the original ECG signals and their MPCs for several beats of the same patient whose representative ECG waveforms are illustrated in Figure 5.1 [201]. The $SL$ values of the normal signals and the ectopic beats exhibit a significant overlap in the range $28 - 35$ [plot (a) in Figure 5.2]. However, the $SL$ values of the MPCs of the PVCs are higher than those of the normal beats, which facilitates their classification [plot (b) in Figure 5.2].

Murthy and Rangaraj [201] applied their QRS detection method (described in Section 4.3.1) to ECG signals of two patients with ectopic beats, and used the $SL$ of MPC to classify the beats with a linear discriminant function (described in Section 9.4.1). They analyzed $208$ beats of the first patient (whose signals are illustrated in Figures 5.1 and 5.2): $132$ out of $155$ normals and $48$ out of $53$ PVCs were correctly classified; one beat was missed by the QRS detection algorithm. Misclassification of normal beats as PVCs was attributed to wider-than-normal QRS complexes and depressed ST segments in some of the normal beats of the patient (see Figure 5.2). The signal of the second patient included 89 normals and 18 PVCs, all of which were detected and classified correctly. It was observed that computation of the MPC was not required in the case of the second patient: The $SL$ values of the original signals provided adequate separation between the normal and ectopic beats. The segments of normal ECG cycles used by Murthy and Rangaraj included the P wave; better results could be obtained by using only the QRS and T waves since most PVCs do not include a distinct P wave and essentially correspond to the QRS and T waves in a normal ECG signal.

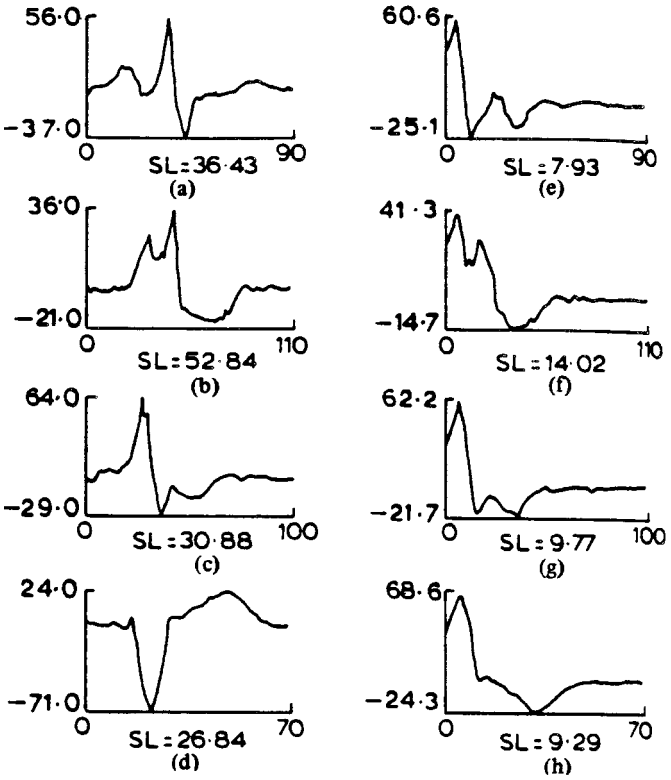


**Figure 5.1** (a) A normal ECG beat and (b)–(d) three ectopic beats (PVCs) of a patient with multiple ectopic foci. (e)–(h) MPCs of the signals in (a)–(d). The $SL$ values of the signals are also indicated [201]. Note that the abscissa is labeled in samples, with a sampling interval of 10 $ms$. The ordinate is not calibrated. The signals have different durations and amplitudes although plotted to the same size. Reproduced with permission from I.S.N. Murthy and M.R. Rangaraj, New concepts for PVC detection, *IEEE Transactions on Biomedical Engineering,* 26(7):409–416, 1979. ©IEEE.

It should be noted that the QRS width may be increased by other abnormal conditions such as bundle-branch block; the definition of $SL$ as above would lead to higher $SL$ for wider-than-normal QRS complexes. Furthermore, ST segment elevation or depression would be interpreted as the presence of energy in the corresponding time interval in the computation of $SL$. Abnormally large T waves could also lead to $SL$ values that are larger than those for normal signals. More sophisticated logic and other parameters in addition to $SL$ could be used to rule out these possibilities and affirm the classification of a beat as an ectopic beat.

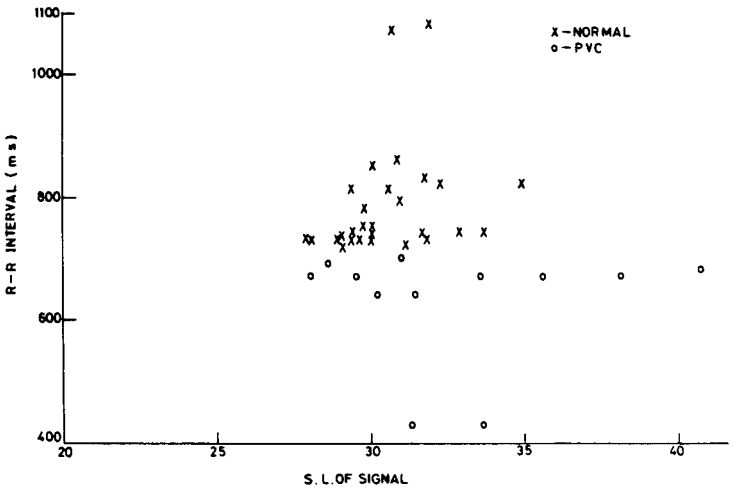


(a)

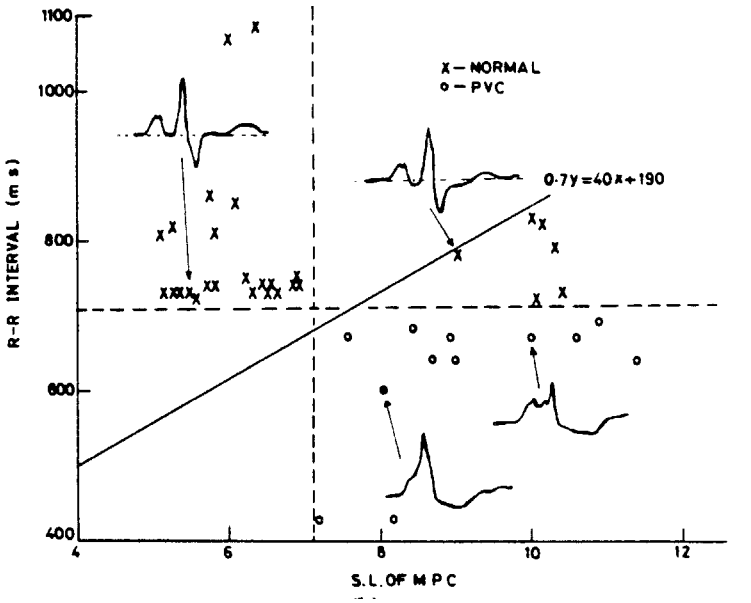


(b)

**Figure 5.2** (a) Plot of $RR$ and $SL$ values of several beats of a patient with multiple ectopic foci (as in Figure 5.1). (b) Same as (a) but with the $SL$ of the MPCs of the signals. A few representative ECG cycles are illustrated. The linear discriminant (decision) function used to classify the beats is also shown [201]. Reproduced with permission from I.S.N. Murthy and M.R. Rangaraj, New concepts for PVC detection, *IEEE Transactions on Biomedical Engineering,* 26(7):409–416, 1979. ©IEEE.

### 5.4.3 ECG waveform analysis

Measures such as the correlation coefficient and $SL$ described in the preceding sections provide general parameters that could assist in comparing waveforms. The representation, however, is in terms of gross features, and many different waveforms could possess the same or similar feature values. Detailed analysis of ECG waveforms will require the use of several features or measurements for accurate categorization of various QRS complex shapes and correlation with cardiovascular diseases. Since the ECG waveform depends upon the lead system used, sets of features may have to be derived for multiple-lead ECGs, including as many as 12 leads that are commonly used in clinical practice.

The steps required for ECG waveform analysis may be expressed as [53]:

1. Detection of ECG waves, primarily the QRS complex, and possibly the P and T waves.
2. Delimitation of wave boundaries, including the P, QRS, and T waves.
3. Measurement of interwave intervals, such as RR, PQ, QT, ST, QQ, and PP intervals.
4. Characterization of the morphology (shape) of the waves.

The last step given above may be achieved using parameters such as the correlation coefficient and $SL$ as described earlier, or via detailed measurements of the peaks of the P, Q, R, S, and T waves (some of which could be negative); the durations of the P, Q, R, S, QRS, and T waves; and the interwave intervals defined above [53]. The nature of the PQ and ST segments, in terms of their being isoelectric or not (in case of the latter, as being positive, negative, elevated, or depressed), should also be documented. However, a large number of such features would make the development of further pattern classification rules difficult.

Cox et al. [53] and Nolle [240] proposed four measures to characterize QRS complexes, as illustrated in Figure 5.3 and defined as follows:

1. *Duration* — the duration or width of the QRS complex.
2. *Height* — the maximum amplitude minus the minimum amplitude of the QRS complex.
3. *Offset* — the positive or negative vertical distance from the midpoint of the baseline to the center of the QRS complex. The baseline is defined as the straight line connecting the temporal boundary points of the QRS complex. The center is defined as the midpoint between the highest and lowest bounds in amplitude of the QRS complex.
4. *Area* — the area under the QRS waveform rectified with respect to a straight line through the midpoint of the baseline.

Since the measures are independent of time, they are not sensitive to the preceding procedures for the detection of fiducial markers.

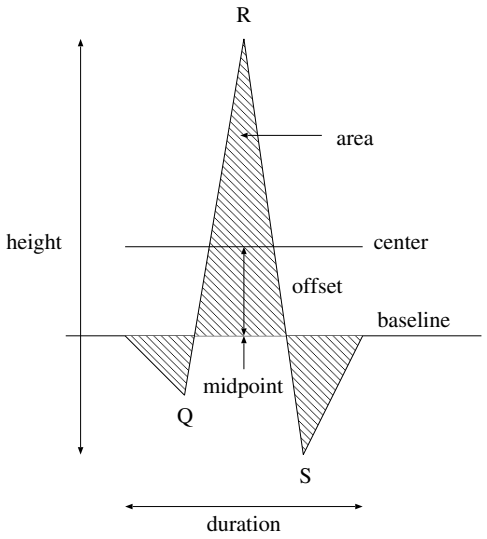


**Figure 5.3** ECG waveform features used by Cox et al. [53] and Nolle [240].

The measures of Cox et al. [53] and Nolle [240] were used to develop a system for arrhythmia monitoring, known as "Argus" for Arrhythmia Guard System, for use in coronary-care units. Figure 5.4 shows the grouping of more than 200 QRS complexes of a patient with multifocal PVCs into 16 dynamic families by Argus using the four features defined above [53]. The families labeled $00, 01, 02, 04, 06$, and $10$ were classified as normal beats by Argus (163 beats which were all classified as normals by a cardiologist; $91\%$ of the normals were correctly labeled by Argus). PVCs of different shapes from more than two ectopic foci form the remaining families, with some of them having shapes close to those of the patient's normal beats. Of the $52$ beats in the remaining families, $96\%$ were labeled as PVCs by the cardiologist; Argus labeled $85\%$ of them as PVCs, $13\%$ as not PVCs, and $2\%$ as borderline beats [240]. Some noteworthy points of one of the clinical tests of Argus with over $50,000$ beats are as follows: $85\%$ of $45,364$ normal beats detected and classified correctly, with $0.04\%$ beats missed; $78\%$ of $4,010$ PVCs detected and classified correctly, with $5.3\%$ beats missed; and $38$ normals (less than $0.1\%$ of the beats) falsely labeled as PVCs.

For recent developments in the analysis and classification of ECG signals, see Ye et al. [241] and Ince et al. [242].

## 5.5 Envelope Extraction and Analysis

Signals with complex patterns such as the EMG and PCG may not permit direct analysis of their waveshape. In such cases, the intricate high-frequency variations may not be of interest; rather, the general trends in the level of the overall activity might

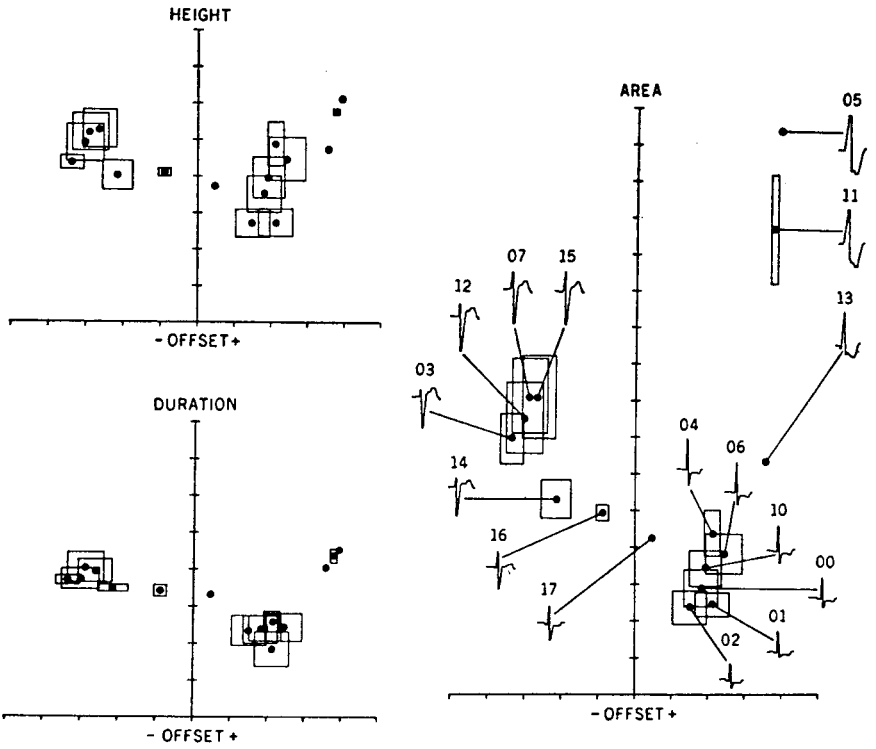


**Figure 5.4** Use of four features to catalog QRS complexes into one of 16 dynamic families of similar complexes enclosed by four-dimensional boxes. The waveforms of typical members of each family are shown in the area-versus-offset feature plane. The family numbers displayed are in the octal (base eight) system. The families labeled $00, 01, 02, 04, 06$, and 10 were classified as normal beats, with the others being PVCs or borderline beats. Reproduced with permission from J.R. Cox, Jr., F.M. Nolle, and R.M. Arthur, Digital analysis of the electroencephalogram, the blood pressure wave, and the electrocardiogram, *Proceedings of the IEEE,* 60(10):1137–1164, 1972. ©IEEE.

convey useful information. Considering, for example, the EMG in Figure 1.18, observe that the general signal level increases with the level of activity (breathing). As another example, the PCG in the case of aortic stenosis, as illustrated in Figure 1.44, demonstrates a diamond-shaped systolic murmur: The *envelope* of the overall signal carries important information. Let us, therefore, consider the problem of extraction of the envelope of a seemingly complex signal.

**Problem:** *Formulate algorithms to extract the envelope of an EMG or PCG signal to facilitate analysis of trends in the level of activity or energy in the signal.*

**Solution:** The first step required in order to derive the envelope of a signal with positive and negative deflections is to obtain the absolute value of the signal at each

time instant, that is, perform full-wave rectification. This procedure will create abrupt discontinuities at time instants when the original signal values change sign, that is, at zero-crossings. The discontinuities create high-frequency components of significant magnitude. This calls for the application of a lowpass filter with a relatively low bandwidth in the range of $0-10$ or $0-50\ Hz$ to obtain smooth envelopes of EMG and PCG signals. An MA filter may be used to perform lowpass filtering, leading to the basic definition of a time-averaged envelope as

$$y(t) = \frac{1}{T_a} \int_{t-T_a}^{t} |x(t)|\, dt, \tag{5.13}$$

where $T_a$ is the duration of the MA filtering window.

In a procedure similar in principle to that described above, Lehner and Rangayyan [131] applied a weighted MA filter to the squared PCG signal to obtain a smoothed energy distribution curve $E(n)$ as

$$E(n) = \sum_{k=1}^{M} x^2(n-k+1)\, w(k), \tag{5.14}$$

where $x(n)$ is the PCG signal, $w(k) = M - k + 1$, and $M = 32$ with the signal sampled at $1,024\ Hz$. Observe that the difference between energy and power is simply a division by the time interval being considered, which may be treated as a scale factor or ignored.

The envelope represents the total averaged activity (such as electrical or acoustic) within the averaging window. An improved filter such as a Bessel filter [40] may be required if a smooth envelope is desired. The filter should strike a balance between the need to smooth discontinuities in the rectified signal and the requirement to maintain good sensitivity to represent relevant changes in signal level or amplitude. This procedure is known as envelope detection or amplitude demodulation. A few related procedures and techniques are described in the following sections.

### 5.5.1 Amplitude demodulation

Amplitude modulation (AM) of signals for radio transmission involves multiplication of the signal $x(t)$ to be transmitted by the carrier $\cos(\omega_c t)$, where $\omega_c$ is the carrier frequency [1–3]. The AM signal is given as $y(t) = x(t)\cos(\omega_c t)$. If the exact carrier wave used at the transmitting end were available at the receiving end as well (including the phase), *synchronous demodulation* becomes possible by multiplying the received signal $y(t)$ with the carrier. We then have the demodulated signal as

$$x_d(t) = y(t)\cos(\omega_c t) = x(t)\cos^2(\omega_c t) = \frac{1}{2}x(t) + \frac{1}{2}x(t)\cos(2\omega_c t). \tag{5.15}$$

The AM component at $2\omega_c$ may be removed by a lowpass filter, which will leave us with the desired signal $x(t)$.

If $x(t)$ is always positive, or a DC bias is added to meet this requirement, it becomes readily apparent that the envelope of the AM signal is equal to $x(t)$. A simple *asynchronous demodulation* procedure that does not require the carrier then becomes feasible: We only need to follow the envelope of $y(t)$. Given that the carrier frequency $\omega_c$ is far greater than the maximum frequency present in $x(t)$, the positive envelope of $y(t)$ may be extracted by performing half-wave rectification. A lowpass filter with an appropriate time constant to "fill the gaps" between the peaks of the carrier wave will provide a good estimate of $x(t)$. The difference between the use of a full-wave rectifier or a half-wave rectifier (that is, the larger gaps between the peaks of the carrier wave available after the latter type of rectification) can be smoothed over by increasing the time constant of the filter. The main differences between various envelope detectors lie in the way the rectification operation is performed and in the lowpass filter used [1, 3].

In a related procedure known as complex demodulation, a given arbitrary signal is demodulated to derive the time-varying amplitude and phase characteristics of the signal for each frequency (band) of interest [243–245]. In this approach, an arbitrary signal $x(t)$ is expressed as

$$x(t) = a(t)\cos[\omega_o t + \psi(t)] + x_r(t), \tag{5.16}$$

where $\omega_o$ is the frequency of interest; $a(t)$ and $\psi(t)$ are the time-varying amplitude and phase of the component at $\omega_o$, respectively; and $x_r(t)$ is the remainder of the signal $x(t)$ after the component at $\omega_o$ has been removed. It is assumed that $a(t)$ and $\psi(t)$ vary slowly in relation to the frequencies of interest. The signal $x(t)$ may be equivalently expressed in terms of complex exponentials as

$$x(t) = \frac{1}{2}\, a(t)\,[\exp\{j[\omega_o t + \psi(t)]\} + \exp\{-j[\omega_o t + \psi(t)]\}] + x_r(t). \tag{5.17}$$

In the procedure of complex demodulation, the signal is shifted in frequency by $-\omega_o$ via multiplication with $2\exp(-j\omega_o t)$, to obtain the result $y(t)$ as

$$\begin{aligned} y(t) &= 2x(t)\exp(-j\omega_o t) \qquad (5.18)\\ &= a(t)\exp[j\psi(t)] + a(t)\exp\{-j[2\omega_o t + \psi(t)]\} + 2x_r(t)\exp(-j\omega_o t). \end{aligned}$$

The second term in the expression above is centered at $2\omega_o$, whereas the third term is centered at $\omega_o$; only the first term is placed at DC. Therefore, a lowpass filter may be used to extract the first term, to obtain the final result $y_o(t)$ as

$$y_o(t) \approx a(t)\exp[j\psi(t)]. \tag{5.19}$$

The desired entities may then be extracted as $a(t) \approx |y_o(t)|$ and $\psi(t) \approx \angle y_o(t)$.

The frequency resolution of the method depends upon the bandwidth of the lowpass filter used. The procedure may be repeated at every frequency (band) of interest. The result may be interpreted as the envelope of the signal for the specified frequency (band). The method was applied for the analysis of HRV by Shin et al. [243] and for the analysis of heart rate and arterial pressure variability by Hayano et al. [244].

In applying envelope detection to biomedical signals such as the PCG and the EMG, it should be noted that there is no underlying RF carrier wave in the signal: The envelope rides on relatively high-frequency acoustic or electrical activity that has a composite spectrum. The difference in frequency content between the envelope and the "carrier activity" will not be comparable to that in AM. Regardless, we could expect at least a ten-fold difference in frequency content: The envelope of an EMG or PCG signal may have an extremely limited bandwidth of $0 - 20\ Hz$, whereas the underlying signal has components up to at least $200\ Hz$, if not to $1,000\ Hz$. Application of envelope detection to the analysis of EMG related to respiration is illustrated in Section 5.10.

### 5.5.2 Synchronized averaging of PCG envelopes

The ECG and PCG form a good signal pair for synchronized averaging: The latter could be averaged over several cardiac cycles using the former as the trigger. However, the PCG is not amenable to direct synchronized averaging as the vibration waves may interfere in a destructive manner and cancel themselves out. Karpman et al. [246] proposed to first rectify the PCG signal, smooth the result using a low-pass filter, and then perform synchronized averaging of the nonnegative envelopes so obtained using the ECG as the trigger. The PCG envelopes were averaged over up to $128$ cardiac cycles to get repeatable averaged envelopes. It should noted that while synchronized averaging can reduce the effects of noise, breathing, coughing, and other types of artifacts, it can also smudge the time boundaries of cardiac events if the heart rate is not constant during the averaging procedure.

Figure 5.5 illustrates the envelopes obtained for a normal case and seven cases of systolic murmur due to various cardiovascular diseases and defects. The typical diamond-shaped envelope in the case of aortic stenosis results in an envelope shaped like an isosceles triangle due to rectification. Mitral regurgitation results in a rectangular holosystolic (spanning the entire systolic period) murmur envelope.

Karpman et al. analyzed $400$ cases of systolic murmurs due to six types of diseases and defects, and obtained an accuracy of $89\%$ via envelope analysis. They proposed a decision tree to classify systolic murmurs based upon the shape of a given murmur's envelope as well as its relation to S1 and S2, which is illustrated in Figure 5.6.

### 5.5.3 The envelogram

Sarkady et al. [227] proposed a Fourier-domain algorithm to obtain envelopes of PCG signals. They defined the *envelogram estimate* as the magnitude of the analytic signal $y(t)$ formed using the PCG, $x(t)$, and its Hilbert transform, $x_H(t)$, as

$$y(t) = x(t) + jx_H(t). \tag{5.20}$$

(*Note:* An analytic function is a complex function of time having a Fourier transform that vanishes for negative frequencies [6, 174].) The Hilbert transform of a signal is

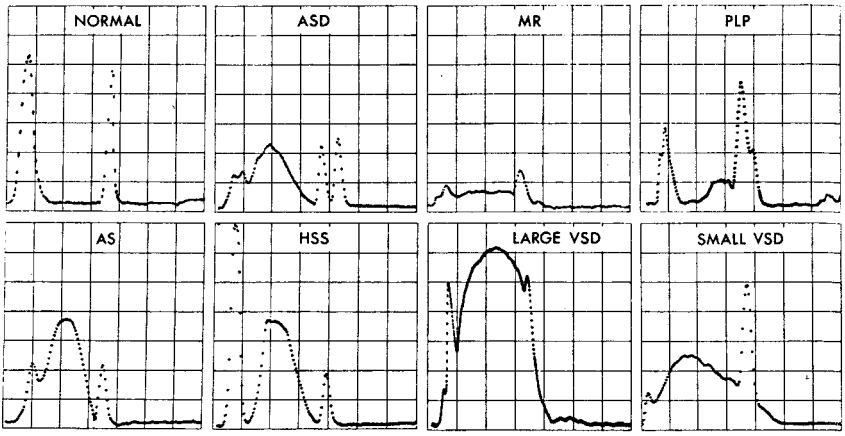


**Figure 5.5** Averaged envelopes of the PCG signals of a normal subject and patients with systolic murmur due to aortic stenosis (AS), atrial septal defect (ASD), hypertrophic subaortic stenosis (HSS), rheumatic mitral regurgitation (MR), ventricular septal defect (VSD), and mitral regurgitation with posterior leaflet prolapse (PLP). Reproduced with permission from L. Karpman, J. Cage, C. Hill, A.D. Forbes, V. Karpman, and K. Cohn, Sound envelope averaging and the differential diagnosis of systolic murmurs, *American Heart Journal,* 90(5):600–606, 1975. ©American Heart Association.

defined as the convolution of the signal with $\frac{1}{\pi t}$, that is,

$$x_H(t) = \int_{-\infty}^{\infty} \frac{x(\tau)}{\pi(t-\tau)}\, d\tau. \tag{5.21}$$

The Fourier transform of $\frac{1}{\pi t}$ is $-j\ \mathrm{sgn}(\omega)$, where

$$\mathrm{sgn}(\omega) = \begin{cases} -1 & \omega < 0 \\ 0 & \omega = 0 \\ 1 & \omega > 0 \end{cases}, \tag{5.22}$$

is the signum function. Then, we have $Y(\omega) = X(\omega)[1 + \mathrm{sgn}(\omega)]$. $Y(\omega)$ is a one-sided or single-sideband function of $\omega$ containing only positive-frequency terms.

Based upon the definitions and properties described above, Sarkady et al. [227] proposed the following algorithm to obtain the envelogram estimate:

1. Compute the DFT of the PCG signal.
2. Set the negative-frequency terms to zero; that is, $X(k) = 0$ for $\frac{N}{2}+2 \le k \le N$, with the DFT indexed $1 \le k \le N$.
3. Multiply the positive-frequency terms, that is, $X(k)$ for $2 \le k \le \frac{N}{2} + 1$, by 2; the DC term $X(1)$ remains unchanged.

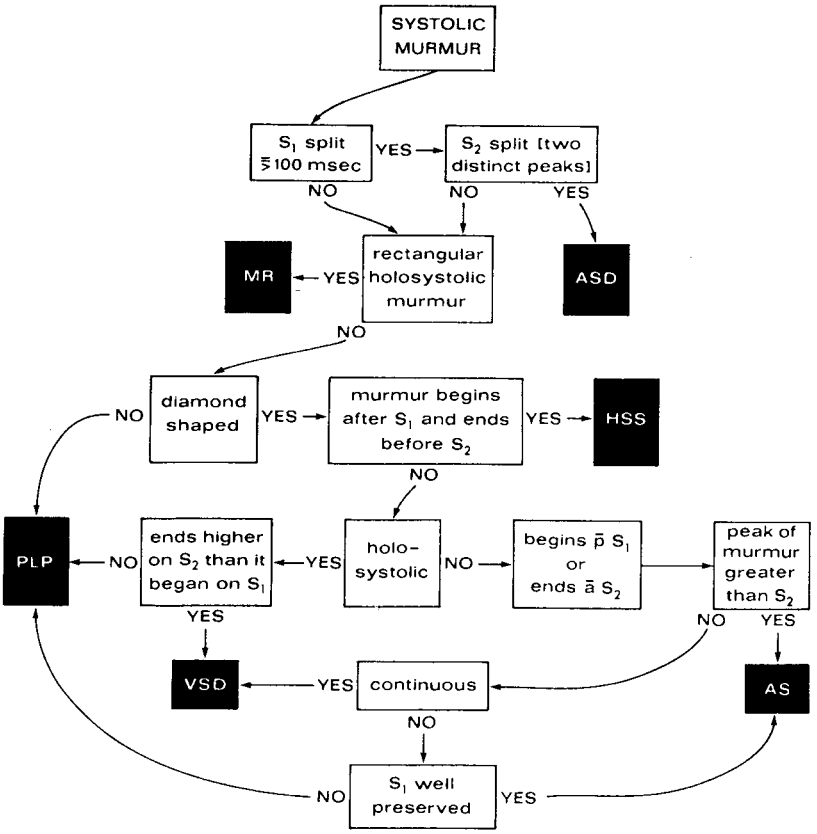


**Figure 5.6** Decision tree to classify systolic murmurs based upon envelope analysis. For details on the abbreviations used, refer to the caption of Figure 5.5. $\bar{p}S_1$, after $S_1$; $\bar{a}S_2$, before $S_2$. Reproduced with permission from L. Karpman, J. Cage, C. Hill, A.D. Forbes, V. Karpman, and K. Cohn, Sound envelope averaging and the differential diagnosis of systolic murmurs, *American Heart Journal,* 90(5):600–606, 1975. ©American Heart Association.

4. Compute the inverse DFT of the result.

5. Obtain an estimate of the envelogram as the magnitude of the result.

The procedure described above, labeled also as complex demodulation by Sarkady et al., yields a high-resolution envelope of the input signal. Envelograms and PSDs computed from PCG signals over single cardiac cycles tend to be noisy and are affected by respiration and muscle noise. Sarkady et al. recommended synchronized averaging of both envelograms and PSDs of PCGs over several cycles. A similar method was used by Baranek et al. [228] to obtain the envelopes of PCG signals for the detection of the aortic component A2 of S2.

See Guerrero et al. [121] for illustrations of the use of the Hilbert transform to obtain envelopes of BCG signals and their application to detect sleep-related breathing disorders.

**Illustration of application:** The topmost plots in Figures 5.7 and 5.8 show one cycle each of the PCG signals of a normal subject and of a patient with systolic murmur, split S2, and opening snap of the mitral valve. The PCG signals were segmented by using the Pan–Tompkins method to detect the QRS complexes in the ECG signal, as illustrated in Figures 4.30 and 4.31 for the same signals. The envelograms of the PCG cycles illustrated and the averaged envelograms (over 16 beats for the normal case and 26 beats for the case with murmur) obtained using the method of Sarkady et al. [227] are shown in the second and third plots of Figures 5.7 and 5.8, respectively. Observe that while a split S2 is visible in the individual signal and envelogram illustrated in Figure 5.7, the split is not clearly seen in the averaged envelogram and envelope, due to variations related to breathing over the duration of the signal and averaging.

Furthermore, based upon the method of Karpman et al. [246], the averaged envelopes were computed by taking the absolute value of the signal over each cardiac cycle, smoothing with a Butterworth lowpass filter with $N = 8$ and $f_c = 50\ Hz$, and synchronized averaging. The last plots in Figures 5.7 and 5.8 show the averaged envelopes. (The Butterworth filter has introduced a small delay in the envelope.) The averaged envelograms and averaged envelopes for the normal case display the envelopes of S1 and S2; the individual components of S1 and S2 have been smoothed over and merged in the averaged results. The averaged envelograms and averaged envelopes for the case with murmur clearly demonstrate the envelopes of S1, the systolic murmur, the split S2, and the opening snap of the mitral valve.

## 5.6 Analysis of Activity

**Problem:** *Propose measures of waveform complexity or activity that may be used to analyze the extent of variability in signals such as the PCG and EMG.*

**Solution:** The samples of a given EMG or PCG signal may, for the sake of generality, be treated as a random variable $x$. Then, the variance $\sigma_x^2 = E[(x - \mu_x)^2]$ represents an averaged measure of the variability or *activity* of the signal about its mean. If the signal has zero mean, or is preprocessed to meet the same condition, we have $\sigma_x^2 = E[x^2]$; that is, the variance is equal to the average power of the signal. Taking the square root, we get the $SD$ of the signal as equal to its $RMS$ value. Thus, the $RMS$ value could be used as an indicator of the level of activity about the mean of the signal. A much simpler indicator of activity is the number of zero-crossings within a specified interval; the zero-crossing rate ($ZCR$) increases as the high-frequency content of the signal increases. A few measures related to the concepts introduced above are described in the following sections, with illustrations of application.

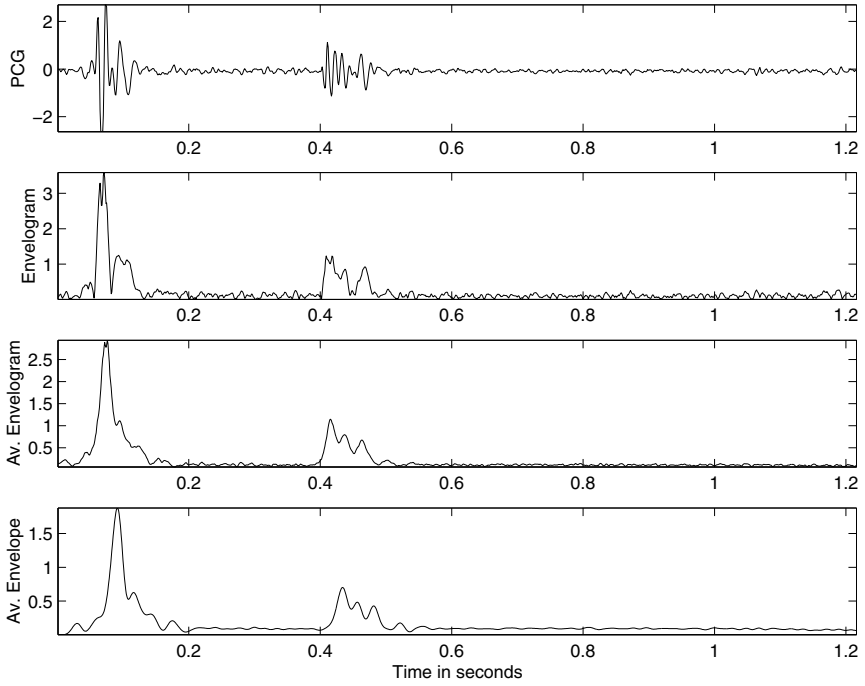


**Figure 5.7** Top to bottom: PCG signal of a normal subject (male, 23 years); envelogram estimate of the signal shown; averaged envelogram over 16 cardiac cycles; averaged envelope over 16 cardiac cycles. The PCG signal starts with S1. See Figure 4.30 for an illustration of segmentation of the same signal. Av. stands for average.

### 5.6.1 The $RMS$ value

The $RMS$ value of a signal $x(n)$ over its total duration of $N$ samples is given by

$$RMS = \left[\frac{1}{N}\sum_{n=0}^{N-1} x^2(n)\right]^{\frac{1}{2}}. \tag{5.23}$$

This global measure of signal level (related to power), however, is not useful for the analysis of trends in nonstationary signals. A running estimate of the $RMS$ value of the signal computed over a causal window of $M$ samples, defined as

$$RMS(n) = \left[\frac{1}{M}\sum_{k=0}^{M-1} x^2(n-k)\right]^{\frac{1}{2}}, \tag{5.24}$$

could serve as a useful indicator of the average power of the signal as a function of time. The duration of the window $M$ needs to be chosen in accordance with the bandwidth of the signal, with $M << N$. Such an approach for computing

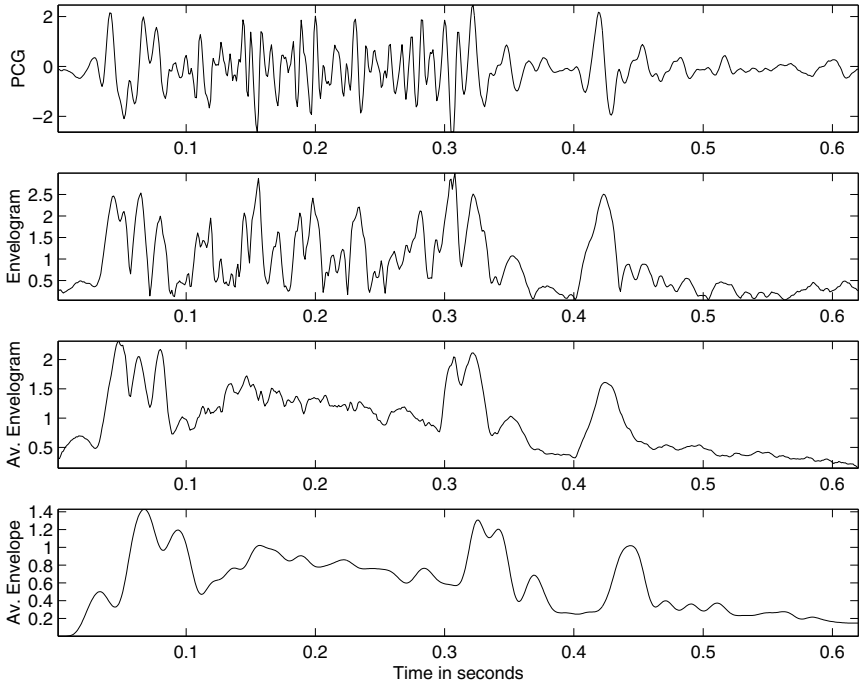


**Figure 5.8** Top to bottom: PCG signal of a patient (female, 14 months) with systolic murmur (approximately $0.1 - 0.28$ $s$), split S2 ($0.28 - 0.38$ $s$), and opening snap of the mitral valve ($0.38 - 0.43$ $s$); envelogram estimate of the signal shown; averaged envelogram over 26 cardiac cycles; averaged envelope over 26 cardiac cycles. The PCG signal starts with S1. Av. stands for average. See Figure 4.31 for an illustration of segmentation of the same signal.

running parameters of signals falls under the general scheme of *short-time analysis* of nonstationary signals [79].

Gerbarg et al. [247, 248] derived power-versus-time curves of PCG signals by computing the average power in contiguous segments of duration $10$ $ms$, and they used the curves to identify systolic and diastolic segments of the signals. They noted that within an interval of $10$ $s$ of a PCG signal, at least one diastolic segment would be longer than the corresponding systolic segment, and that all systolic segments in the interval would have approximately the same duration. Innocent (physiological) systolic murmurs in children were observed to be limited to the first and middle thirds of the systolic interval between S1 and S2, whereas pathological systolic murmurs due to mitral regurgitation were noted to be holosystolic. Based upon these observations, Gerbarg et al. computed ratios of the mean power of the last third of systole to the mean power of systole and also to a certain "standard" noise level. A ratio was also computed of the mean energy of systole to the mean energy of the PCG over the complete cardiac cycle. Agreement in the range of $78 - 91\%$ was

obtained between computer classification based upon the three ratios defined above and clinical diagnosis of mitral regurgitation in different groups of subjects.

Use of the $RMS$ value for the analysis of EMG and VMG signals, and thereby analysis of muscular activity, is illustrated in Section 5.11.

### 5.6.2 Zero crossing rate

An intuitive indication of the "busy-ness" of a signal is provided by the number of times it crosses the zero-activity line or some other reference level. $ZCR$ is defined as the number of times the signal crosses the reference within a specified interval. However, $ZCR$ could be easily affected by DC bias, baseline wander, and low-frequency artifacts. For these reasons, it would be advisable to measure the $ZCR$ of the derivative of the signal, which would be similar to the definition of turning points in the test for randomness described in Section 3.2.1. Saltzberg and Burch [249] discuss the relationship between $ZCR$ and moments of PSDs, and their application to EEG analysis.

In spite of its simplicity, $ZCR$ has been used in practical applications such as speech signal analysis to perform speech-versus-silence decision and to discriminate between voiced and unvoiced sounds [79] (see also Figure 3.1), and PCG analysis for the detection of murmurs. Jacobs et al. [250] used $ZCR$ to perform normal-versus-abnormal classification of PCG signals using the ECG as a trigger, and obtained correct classification rates of $95\%$ for normals $(58/61)$ and $94\%$ for abnormals $(77/82)$. They indicated a decision limit of $20$ zero-crossings in a cardiac cycle. Yokoi et al. [251] proposed a screening system based upon measurements of the maximum amplitude and $ZCR$ in $8\ ms$ segments of PCG signals (sampled at $2\ kHz$). They obtained correct classification rates of $98\%$ with $4,809$ normal subjects and $76\%$ with $1,217$ patients with murmurs.

### 5.6.3 Turns count

Willison [252] proposed to analyze the level of activity in EMG signals by determining the number of spikes occurring in the interference pattern (see also Goodgold and Eberstein [30], Fuglsang-Frederiksen and Månsson [253], and Dowling et al. [254]). Instead of counting zero-crossings, Willison's method investigates the significance of every change in phase (direction or slope) of the EMG signal called a *turn*. Turns greater than $100\ \mu V$ are counted, with the threshold selected so as to avoid counting insignificant fluctuations due to noise. The method is similar to counting turning points as in the test for randomness described in Section 3.2.1, but is expected to be robust in the presence of noise due to the threshold imposed. The method is not directly sensitive to SMUAPs, but significant phase changes caused by superimposed SMUAPs are counted. Willison [252] found that EMG signals of subjects with myopathy possessed higher turns counts than those of normal subjects at comparable levels of volitional effort.

**Illustration of application:** The topmost plot in Figure 5.9 illustrates the EMG signal over two breath cycles from the crural diaphragm of a dog recorded via im-

planted fine-wire electrodes [40]. The subsequent plots illustrate, in top-to-bottom order, the short-time $RMS$ values, the turns count by Willison's procedure, and the smoothed envelope of the signal. The $RMS$ and turns count values were computed using a causal moving window of duration 70 $ms$ (210 samples). The window duration needs to be chosen to strike a balance between the extent of smoothing desired in the turns count series and the accuracy in reflecting the nonstationary nature of the signal; in the present example, nonstationarity is related to the increasing level of EMG activity with inspiration. The envelope was obtained by taking the absolute value of the signal (equivalent to full-wave rectification) followed by a Butterworth lowpass filter of order $N = 8$ and cutoff frequency $f_c = 8\ Hz$. It is seen that all three of the derived features demonstrate the expected increasing trend with the level of contraction (breath), and can serve as correlates or indicators of muscle contraction and the concomitant EMG complexity. The results may be further smoothed (lowpass filtered) if desired.

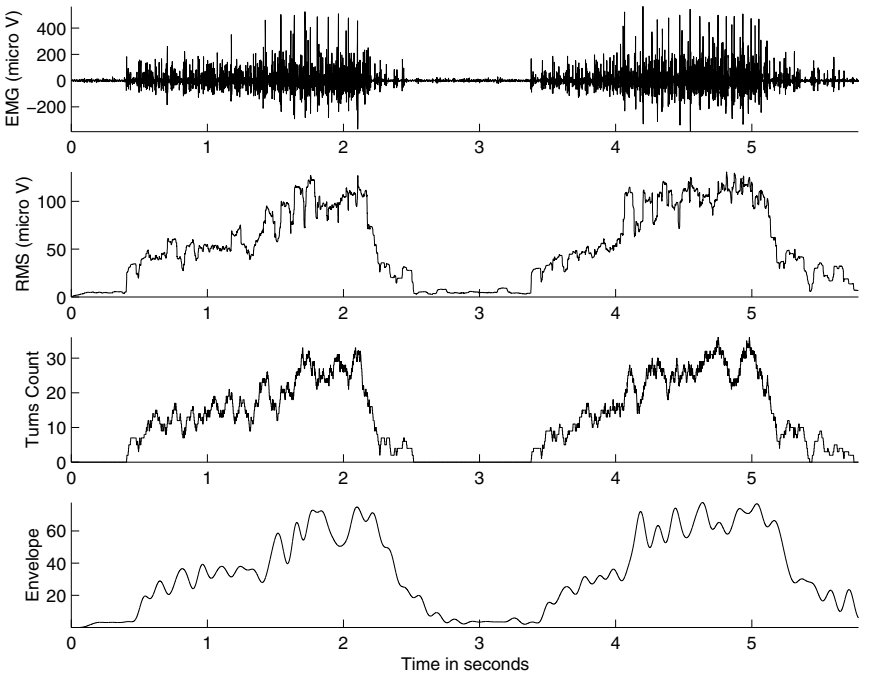


**Figure 5.9** Top to bottom: EMG signal over two breath cycles from the crural diaphragm of a dog recorded via implanted fine-wire electrodes; short-time $RMS$ values; turns count using Willison's procedure; and smoothed envelope of the signal. The $RMS$ and turns count values were computed using a causal moving window of 70 $ms$ duration. EMG signal courtesy of R.S. Platt and P.A. Easton, Department of Clinical Neurosciences, University of Calgary.

Figure 5.10 illustrates one 70 $ms$ segment of the EMG signal in Figure 5.9 with the boundary points of the significant turns as detected by Willison's proce-

dure marked by the '*' symbol. The procedure was implemented by first computing the derivative of the EMG signal and detecting points of change in its sign. A turn was marked wherever the EMG signal differed by at least $100\ \mu V$ between successive points of sign change in the derivative. Observe from Figure 5.10 that the EMG signal need not cross the zero line to cause a turns count, and that zero-crossings with voltage swings of less than $100\ \mu V$ are not counted as turns.

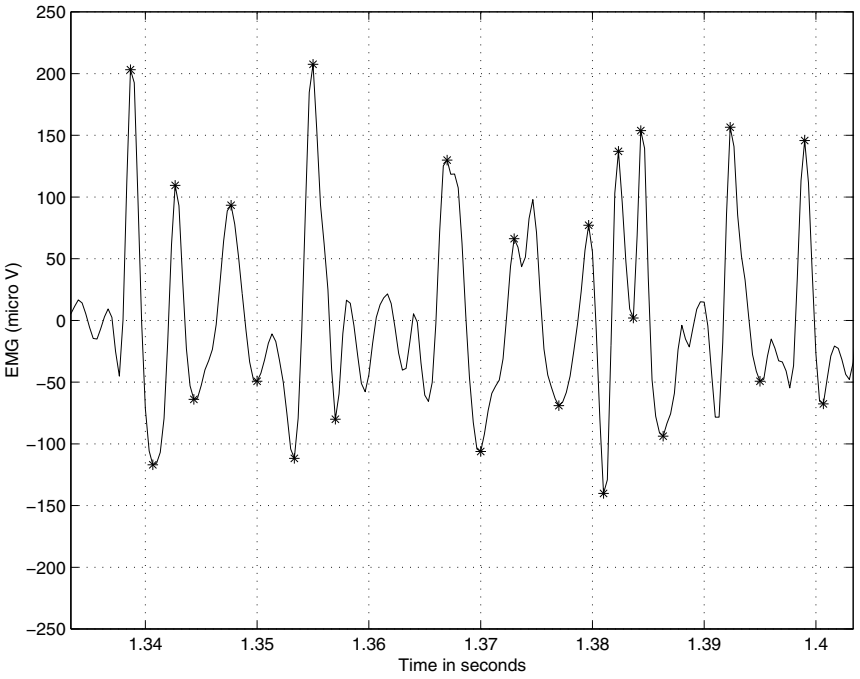


**Figure 5.10** Illustration of the detection of turns in a $70\ ms$ window of the EMG signal in Figure 5.9. The segments of the signal between pairs of '*' marks have been identified as significant turns.

### 5.6.4 Form factor

Based upon the notion of variance as a measure of signal activity, Hjorth [255–257] (see also Cooper et al. [54]) proposed a method for the analysis of EEG waves. In this method, short-time segments of duration $1\ s$ or longer are analyzed and three parameters are computed. The first parameter is called *activity* and is simply the variance $\sigma_x^2$ of the signal segment $x(n)$. The second parameter, called *mobility* $M_x$, is computed as the square root of the ratio of the activity of the first derivative of the

signal to the activity of the (original) signal:

$$M_x = \left[\frac{\sigma_{x'}^2}{\sigma_x^2}\right]^{\frac{1}{2}} = \frac{\sigma_{x'}}{\sigma_x}, \tag{5.25}$$

where $x'$ stands for the first derivative of $x$. The third parameter, called *complexity* or the *form factor* ($FF$), is defined as the ratio of the mobility of the first derivative of the signal to the mobility of the signal itself:

$$FF = \frac{M_{x'}}{M_x} = \frac{\sigma_{x''}/\sigma_{x'}}{\sigma_{x'}/\sigma_x}, \tag{5.26}$$

where $x''$ stands for the second derivative of the signal. The complexity of a sinusoidal wave is unity; other waveforms have complexity values increasing with the extent of variations present in them.

Hjorth [256, 257] described the mathematical relationships between the activity, mobility, complexity, and PSD of a signal, and applied them to model EEG signal generation. Binnie et al. [258, 259] described the application of $FF$ and spectrum analysis to EEG analysis for the detection of epilepsy. However, because the computation of $FF$ is based upon the first and second derivatives of the signal and their variances, the measure is sensitive to noise. A complex and relatively wideband signal such as the EMG is not amenable to analysis via $FF$. Application of $FF$ to discriminate between normal and ectopic ECG beats is illustrated in Section 5.7.

We have explored a few measures to characterize waveform complexity in this section. Many authors have proposed several other diverse measures and interpretations of waveform or system complexity in the literature, examples of which include features based upon nonlinear dynamics and the correlation dimension [260], and the embedding dimension of time-varying dynamic systems [261].

## 5.7 Application: Parameterization of Normal and Ectopic ECG Beats

**Problem:** *Develop a parameter to discriminate between normal ECG waveforms and ectopic beats (PVCs).*

**Solution:** We have observed several times that ectopic beats, due to the abnormal propagation paths of the associated excitation pulses, typically possess waveforms that are significantly different from those of the normal QRS waveforms of the same subject. More often than not, ectopic beats have bizarre and complex waveshapes. The form factor $FF$ described in Section 5.6.4 parameterizes the notion of waveform complexity, providing a value that increases with complexity. Therefore, $FF$ appears to be a suitable measure to discriminate between normal and ectopic beats. Note that the $RR$ interval by itself cannot indicate ectopic beats, as the $RR$ interval could vary due to sinus arrhythmia and conduction problems, as well as due to HRV.

Figure 5.11 displays a segment of the ECG of a patient with ectopic beats; the segment illustrates the initiation of an episode of *ventricular bigeminy*, where every normal beat is followed by an ectopic beat [33]. The ECG of the patient was

processed using the Pan–Tompkins algorithm for QRS detection (see Section 4.3.2). QRS marker points were detected using a simple threshold applied to the output of the Pan–Tompkins algorithm. Each beat was segmented at points $160\ ms$ before and $240\ ms$ after the detected marker point; the diamond and circle symbols on the ECG in Figure 5.11 indicate the starting and ending points of the corresponding beats. The $FF$ value was computed for each segmented beat. The $RR$ interval (in $ms$) and the $FF$ value are shown for each beat in Figure 5.11. It can be readily seen that the $FF$ values for the PVCs are higher than those for the normal beats.

Note from Figure 5.11 that the $RR$ intervals for the PVCs are lower than those for the normal beats, and that the normal beats that follow the PVCs have higher-than-normal $RR$ intervals due to the compensatory pause. Pattern classification of the ECG beats in this example as normal or PVCs using $RR$ and $FF$ is described in Section 9.11.

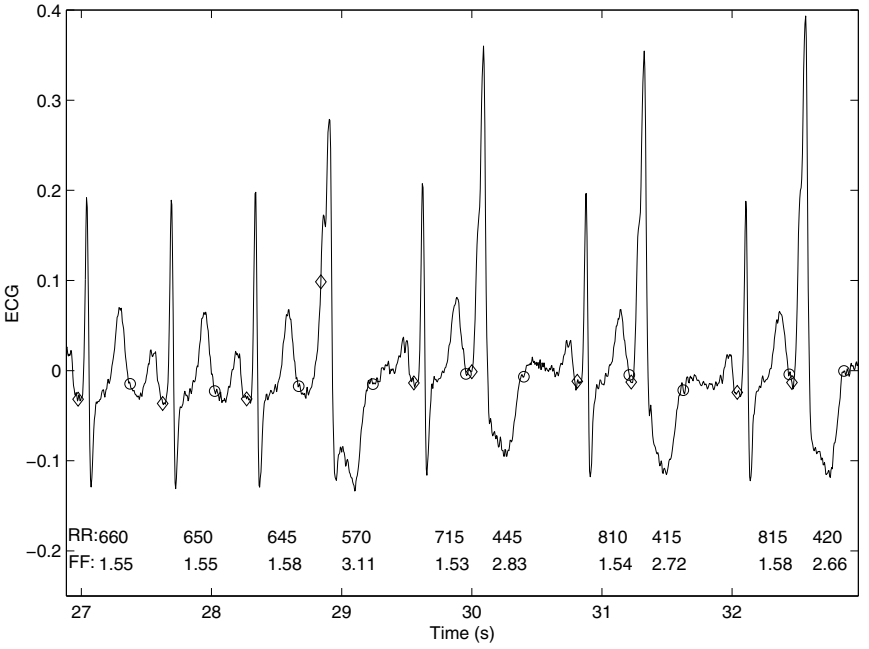


**Figure 5.11** Segment of the ECG of a patient (male, $65$ years) with ectopic beats. The diamond and circle symbols indicate the starting and ending points, respectively, of each QRS-T wave obtained using the Pan–Tompkins algorithm. The $RR$ interval (in $ms$) and the $FF$ value are shown for each beat.

## 5.8 Application: Analysis of Exercise ECG

**Problem:** *Develop an algorithm to analyze changes in the ST segment of the ECG during exercise.*

**Solution:** Hsia et al. [262] developed a method to analyze changes in the ST segment of the ECG signal while the subject performed physical exercises. The analysis was performed as part of a radionuclide ventriculography (gated blood-pool imaging) procedure. In this procedure, nuclear medicine images are obtained of the left ventricle before and after the patient performs exercises on a treadmill or bicycle ergometer. Images are obtained at different phases of the cardiac cycle by gating the radionuclide (gamma ray) emission data with reference to the ECG; image data for each phase are averaged over several cardiac cycles [18]. Analysis of exercise ECG is complicated due to baseline artifacts caused by the effects of respiration, skin resistance changes due to perspiration, and soft tissue movement affecting electrode contact. Detection of changes in the ST segment in the presence of such artifacts poses a major challenge.

One of the main parameters used by Hsia et al. is related to the correlation coefficient as defined in Equation 3.96. The measure, however, is affected by baseline variations. To address this, a modified correlation coefficient was defined as

$$\gamma_{xy} = \frac{\sum_{n=0}^{N-1}[x(n)][y(n)-\Delta]}{\sqrt{\sum_{n=0}^{N-1}[x(n)]^2 \sum_{n=0}^{N-1}[y(n)-\Delta]^2}}. \tag{5.27}$$

Here, $x(n)$ is the template, $y(n)$ is a segment of the ECG signal being analyzed, $\Delta$ is a baseline correction factor defined as the difference between the baseline of $y(n)$ and the baseline of $x(n)$, and $N$ is the duration (number of samples) of the template and the signal segment being analyzed. The template was generated by averaging up to 20 QRS complexes that met a specified $RR$ interval constraint.

Hsia et al. proposed a method to establish the baseline of each ECG beat by searching for the PQ segment by backtracking from the detected R point (trigger for gating the image data). The region of three consecutive samples with the minimum change (maximum flatness) preceding the QRS was taken to represent the baseline of the beat. (*Note:* The PQ segment is almost always isoelectric, whereas the ST segment is variable in the presence of cardiac diseases.) The search procedure also established the width of the QRS complex to be used in template matching ($N$ in Equation 5.27). Beats with $\gamma_{xy} < 0.85$ were considered to be abnormal. The baseline correction factor in Equation 5.27 provided the robustness required.

Groups of 16 successive normal beats were aligned and averaged to obtain a representative waveform. The ST segment level was computed as the difference between a reference ST point and the isoelectric level of the current averaged beat. The averaging procedure included a condition to reject beats with abnormal morphology, such as PVCs. The ST reference point was defined as $R + 64\ ms + \max(4, \frac{200-HR}{16}) \times 4\ ms$ or $S + 44\ ms + \max(4, \frac{200-HR}{16}) \times 4\ ms$, where $R$ or $S$ indicates the position of the R or S wave of the present beat in $ms$, and $HR$ is in $bpm$. Significant ST level differences were reported by the algorithm. (Elevation or depression of the ST segment by more than $0.1\ mV$ with reference to the baseline is considered to be significant.) Furthermore, the slope of the ST segment was computed by using two samples before and two samples after the detected ST point as described above (a duration of $16\ ms$, with the sampling rate of $250\ Hz$).

In addition to the analysis of the ST segment, the method of Hsia et al. performed rhythm analysis, identified PVCs and other abnormal beats, and assisted in the rejection of radionuclide emission data related to abnormal beats from the imaging procedure. The combined use of nuclear medicine imaging and ECG analysis can improve the accuracy of the diagnosis of myocardial ischemia.

## 5.9 Application: Quantitative Analysis of the EMG in Relation to Force Exerted

**Problem:** *Propose methods for parametric analysis of the variations in the EMG signal with respect to the force exerted by a muscle.*

**Solution:** We have seen several examples demonstrating increasing levels of power and complexity of the EMG signal with increasing muscular activity or force exerted; see, for example, Figures 1.18, 1.19, 1.20, and 5.9. We have also studied how such variations in a signal may be represented quantitatively using measures such as the $RMS$ value, $ZCR$, and turns count. Let us now explore the relationships between these entities in a formal and mathematical manner.

Figure 5.12 shows the ECG and force signals as in Figure 1.20, but with automatic delineation of the portions of the force signal corresponding to the five intervals of muscular contraction. To perform this task, starting from the first sample, the point where the force signal increased beyond $10\%$ MVC was identified. Then, the next point where the signal dropped below $10\%$ MVC was identified. This process was repeated until the end of the signal. To refine the definition of each interval of contraction, a threshold was defined as $0.7$ times the maximum level of contraction within the interval. Then, the smaller extent of each interval previously identified, within which the force remained above the threshold, was detected. The final intervals detected by this procedure are labeled in Figure 5.12 with '*' marks.

Within each interval of the force signal identified as above as well as the corresponding interval in the EMG signal, the average force exerted, the $RMS$ value, $ZCR$, and the turns count divided by the time duration of the interval (referred to as the turns count rate or $TCR$) were computed. The threshold to detect significant turns was set at $100\ \mu V$.

Figure 5.13 demonstrates the important difference between zero-crossings and turns. The cumulative number of zero-crossings detected keeps increasing with time even during the intervals when no muscular force is exerted, due to noisy variations in the EMG signal during the periods of rest. The threshold to detect significant turns, which was set at $100\ \mu V$ in this experiment, disregards the small turns associated with the background variations in the EMG signal, as well as small variations during periods of contraction. Thus, the cumulative number of significant turns detected is seen to increase only during the periods of contraction and not during the periods of rest. Therefore, we may expect $TCR$ to be a better indicator of muscular force exerted than $ZCR$.

In order to analyze the variation of the EMG signal with force in a quantitative manner, a linear fit was computed to represent the variation of each EMG parameter

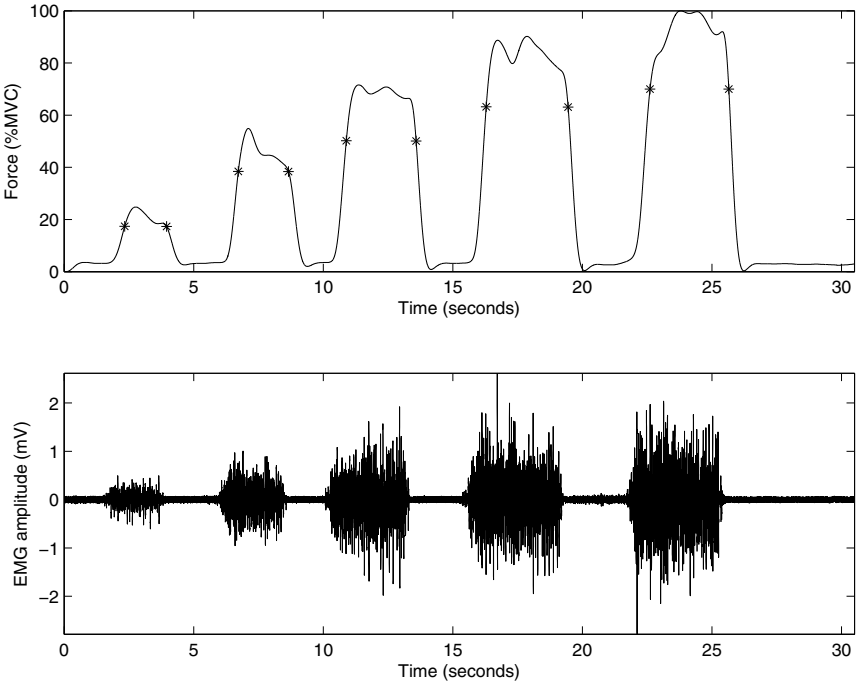


**Figure 5.12** Force and EMG signals recorded from the forearm muscle of a subject using surface electrodes. The portions of muscular contraction have been automatically identified in the force signal and delimited by the '*' marks.

versus force. The linear models (straight-line fits) obtained are shown in the plots in Figures 5.14, 5.15, and 5.16 for the $RMS$, $ZCR$, and $TCR$ values, respectively. To obtain a measure of fit between each parameter and force, the correlation coefficient was computed as

$$r^2 = \frac{\left[\sum_{n=1}^{n=N} x(n)\,y(n) - N\,\bar{x}\,\bar{y}\right]^2}{\left[\sum_{n=1}^{n=N} x^2(n) - N\,\bar{x}^2\right]\;\left[\sum_{n=1}^{n=N} y^2(n) - N\,\bar{y}^2\right]}, \tag{5.28}$$

where $N$ is the number of samples of $x$ or $y$ representing the variables $RMS$, $ZCR$, $TCR$, or force ($N = 5$ in the present study); $\bar{x}$ is the mean of $x$. The values of $r^2$ for $RMS$, $ZCR$, and $TCR$ are given in the captions of Figures 5.14, 5.15, and 5.16, respectively. The value of $ZCR$ shows limited variation and low correlation with force. It is evident that $RMS$ and $TCR$ have a high degree of correlation and linear behavior with respect to force.

The study described above is limited due to the use of a single EMG signal and a simple method to delimit the intervals of muscular contraction. It is seen in Figure 5.12 that the muscular force exerted is not constant within each interval. For

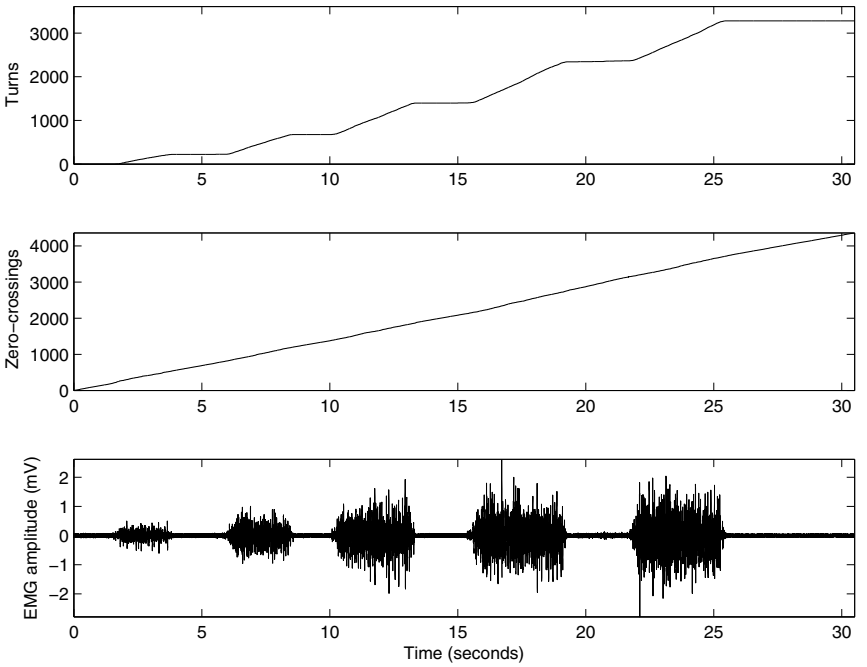


**Figure 5.13** Bottom to top: EMG signal, cumulative count of zero-crossings, and cumulative number of significant turns. See also Figure 5.12.

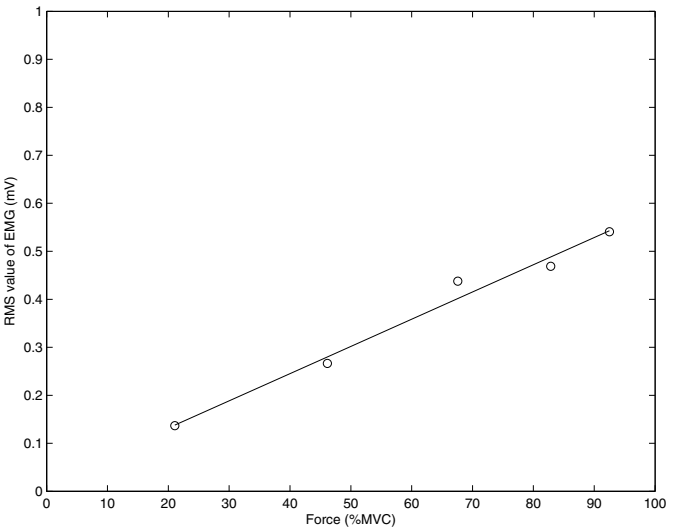


**Figure 5.14** Variation of the $RMS$ value of the EMG signal in Figure 5.12 with the average muscular force exerted in each of the five periods of contraction. The '$\circ$' marks indicate the measured values and the straight line indicates the computed linear model. $r^2 = 0.98$.

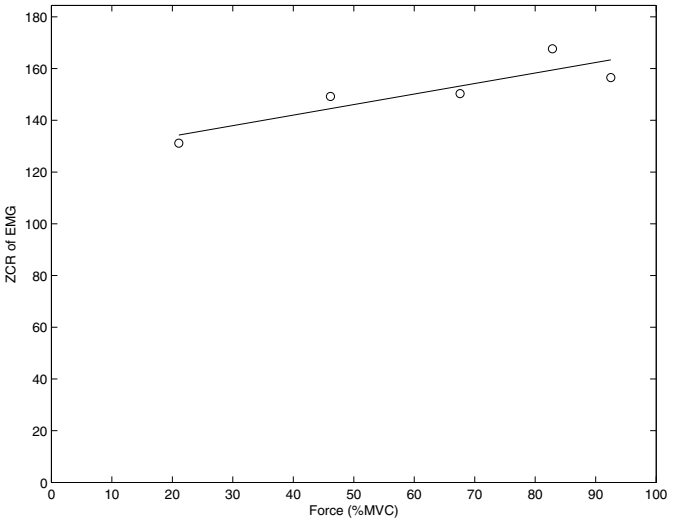


**Figure 5.15** Variation of the $ZCR$ value of the EMG signal in Figure 5.12 with the average muscular force exerted in each of the five periods of contraction. The '$\circ$' marks indicate the measured values and the straight line indicates the computed linear model. $r^2 = 0.78$.

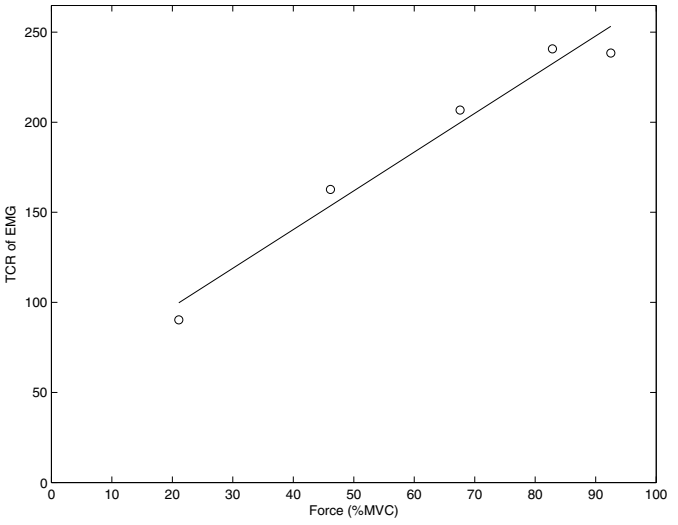


**Figure 5.16** Variation of the $TCR$ value of the EMG signal in Figure 5.12 with the average muscular force exerted in each of the five periods of contraction. The '$\circ$' marks indicate the measured values and the straight line indicates the computed linear model. $r^2 = 0.97$.

robust analysis, it is necessary to repeat the experiment several times with many subjects and analyze a large number of samples of the parameters. See Section 5.11 for further related discussion and illustration of the relationships between EMG and force.

## 5.10 Application: Analysis of Respiration

**Problem:** *Propose a method to relate EMG activity to airflow during respiration.*

**Solution:** Platt et al. [40] recorded EMG signals from the parasternal intercostal and crural diaphragm muscles of dogs. One EMG signal was obtained from a pair of electrodes mounted at a fixed distance of 2 $mm$ placed between fibers in the third left parasternal intercostal muscle about 2 $cm$ from the edge of the sternum. The crural diaphragm EMG was obtained via fine-wire electrodes sewn in-line with the muscle fibers and placed 10 $mm$ apart. During the signal acquisition experiment, the dog breathed through a snout mask, and a pneumotachograph was used to measure airflow. Figures 1.18, 1.19, and 5.9 show samples of the crural EMG signal.

Although the EMG signal is commonly used in many physiological studies including analysis of respiration, the intricate variations in the signal are often not of interest. A measure of the total or integrated electrical activity, ideally reflecting the global activity in the pool of active motor units of the muscle, would serve the purposes of most analyses [40]. As the EMG signal is nonstationary, short-time measures are called for. The smoothed envelope of the EMG signal is commonly used under these circumstances.

Platt et al. observed that the filters commonly used for smoothing rectified EMG signals had poor high-frequency attenuation, resulting in noisy envelopes. They proposed a modified Bessel filter for application to the EMG signal after full-wave rectification; the filter severely attenuated frequencies beyond 20 $Hz$ with gain $< -70\ dB$, and yielded EMG envelopes that were much smoother than those given by other filters.

The EMG envelopes derived by Platt et al. agreed very well with the inspiratory airflow pattern. Figure 5.17 shows plots of the parasternal intercostal EMG signal over two breath cycles, the corresponding filtered envelope, and the airflow pattern. Figure 5.18 shows the correlation between the filtered EMG envelope amplitude and the airflow in liters per second. It is evident that the envelope extracted by this method is an excellent correlate of inspiratory airflow.

## 5.11 Application: Electrical and Mechanical Correlates of Muscular Contraction

**Problem:** *Derive parameters from the electrical and mechanical manifestations of muscular activity that correlate with the level of contraction or force produced.*

**Solution:** Zhang et al. [85, 86] studied the usefulness of simultaneously recorded EMG and VMG signals in the analysis of muscular force produced by contraction.

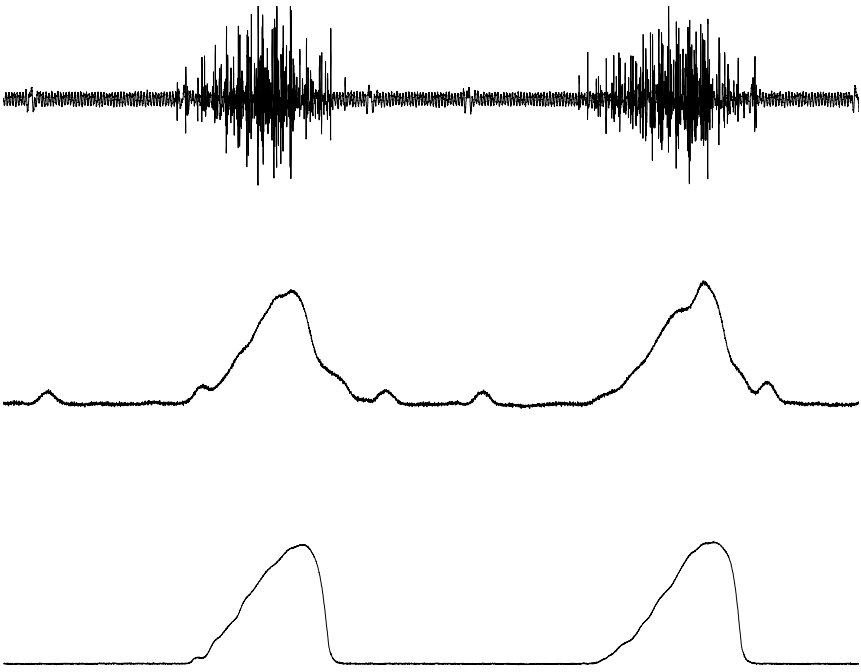

**Figure 5.17** Top to bottom: EMG signal over two breath cycles from the parasternal intercostal muscle of a dog recorded via implanted electrodes; EMG envelope obtained with the modified Bessel filter with a time constant of 100 $ms$; and inspiratory airflow. The duration of the signals plotted is 5 $s$. The several minor peaks appearing in the envelope are related to the ECG which appears as an artifact in the EMG signal. Data courtesy of R.S. Platt and P.A. Easton, Department of Clinical Neurosciences, University of Calgary [40].

In their experimental procedure, the subjects performed isometric contraction (that is, with no movement of the associated leg) of the rectus femoris (thigh) muscle to different levels of torque with a Cybex II dynamometer. Four levels of contraction were performed from 20% to 80% of the MVC level of the individual subject. The experiments were performed at three knee-joint angles of 30°, 60°, and 90°. Each contraction was held for a duration of about 6 $s$, and the subjects rested in between experiments to prevent the development of muscle fatigue. The VMG signal was recorded using a Dytran 3115a accelerometer, and surface EMG signals were recorded using disposable $Ag - AgCl$ electrodes. The VMG signals were filtered to the bandwidth $3 - 100$ $Hz$ and the EMG signals were filtered to $10 - 300$ $Hz$. The VMG and EMG signals were sampled at 250 $Hz$ and $1,000$ $Hz$, respectively. Figure 2.4 illustrates sample recordings of the VMG and EMG signals at two levels of contraction.

$RMS$ values were computed for each contraction level over a duration of 5 $s$. Figure 5.19 shows the variation of the $RMS$ values of the EMG and VMG signals

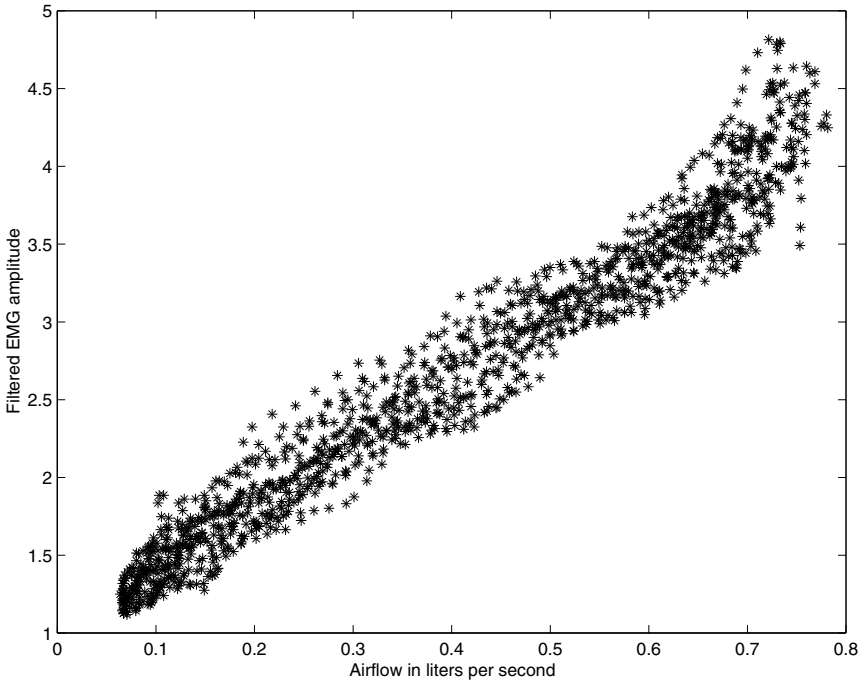


**Figure 5.18** Correlation between EMG amplitude obtained from the Bessel-filtered envelope versus inspiratory airflow. The EMG envelope was filtered using a modified Bessel filter with a time constant of 100 $ms$. Data courtesy of R.S. Platt and P.A. Easton, Department of Clinical Neurosciences, University of Calgary [40].

acquired at a knee-joint angle of $60^\circ$ and averaged over four subjects. The almost-linear trends of the $RMS$ values of both the signals with muscular contraction indicate the usefulness of the derived parameter in the analysis of muscular activity. It should, however, be noted that the relationship between $RMS$ values and contraction may not follow the same (linear) pattern for different muscles. Figure 5.20 shows the $RMS$-versus-%MVC relationships for three muscles: The relationship is linear for the FDI, whereas it is nonlinear for the biceps and deltoid muscles [263].

## 5.12 Application: Statistical Analysis of VAG Signals

**Problem:** *Knee-joint VAG signals possess different levels of waveform complexity depending upon the state of the cartilage covering the joint surfaces. Explore the use of statistical parameters that characterize variability for parametric representation and classification of VAG signals.*

**Solution:** As described in Section 1.2.14, a normal knee joint has smooth cartilage surfaces and produces almost no sound or vibration; see also Section 8.2.3.

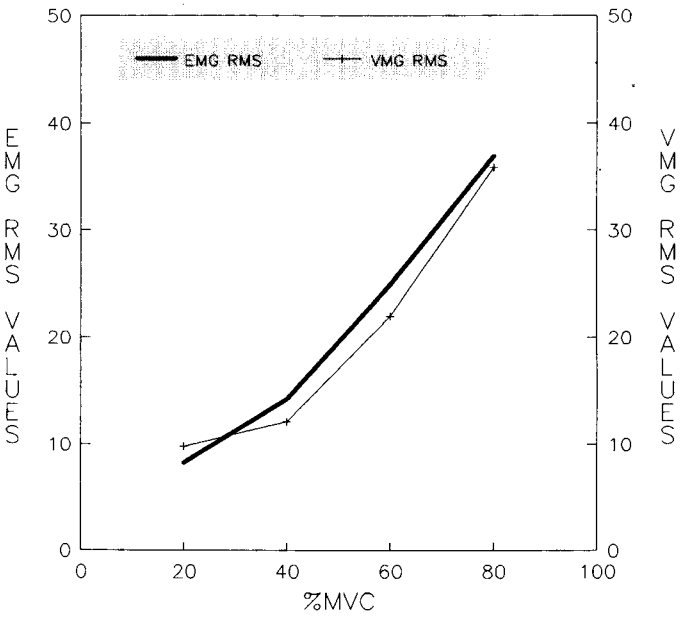


**Figure 5.19** $RMS$ values of the VMG and EMG signals for four levels of contraction of the rectus femoris muscle at $60^\circ$ knee-joint angle averaged over four subjects. Reproduced with permission from Y.T. Zhang, C.B. Frank, R.M. Rangayyan, and G.D. Bell, Relationships of the vibromyogram to the surface electromyogram of the human rectus femoris muscle during voluntary isometric contraction, *Journal of Rehabilitation Research and Development,* 33(4): 395–403, 1996. ©Department of Veterans Affairs.

Regardless, when a VAG signal is recorded from a normal knee joint, a signal with some variations is obtained. Under pathological conditions, the cartilage surfaces are eroded and could generate additional sounds. We could expect the statistics of the variability of normal and abnormal VAG signals to demonstrate differences due to the different nature of the underlying causes. Rangayyan and Wu [264–266] explored the use of several statistical parameters for screening VAG signals. The related background and methods are described in the following paragraphs.

### 5.12.1 Acquisition of knee joint VAG signals

The data set used in the studies of Rangayyan and Wu [264–266] consists of 89 signals, with 51 from normal volunteers (22 male, 29 female, age $28 \pm 9.5$ years) and 38 from subjects with knee-joint pathology (20 male, 18 female, age $35 \pm 13.8$ years). The normal condition of volunteers was established by clinical examination and history. The abnormal signals were collected from symptomatic patients scheduled to undergo arthroscopy independent of the VAG studies. Informed consent was ob-

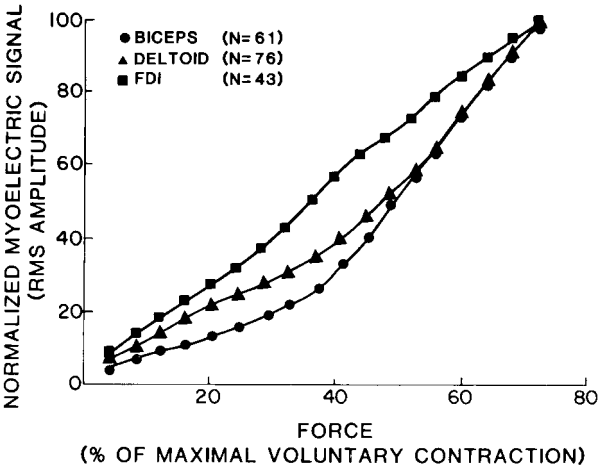


**Figure 5.20** EMG $RMS$ value versus level of muscle contraction expressed as a percentage of MVC for each subject. The relationship is displayed for three muscles. FDI: first dorsal interosseus. N: number of muscles (subjects) in the study. Reproduced with permission from J.H. Lawrence and C.J. de Luca, Myoelectric signal versus force relationship in different human muscles, *Journal of Applied Physiology,* 54(6):1653–1659, 1983. ©American Physiological Society.

tained from each subject. The experimental protocol was approved by the Conjoint Health Research Ethics Board of the University of Calgary.

Each subject sat on a rigid table in a relaxed position with the leg to be tested being freely suspended in air. The VAG signal was recorded by an accelerometer (model 3115a, Dytran, Chatsworth, CA), placed at the midpatella position of the knee, as the subject swung the leg over an approximate angle range of $135^\circ$ (approximately full flexion) to $0^\circ$ (full extension) and back to $135^\circ$ in $4\ s$ [96]. The first half of each VAG signal corresponds, approximately, to extension, and the second half corresponds to flexion of the leg. The VAG signals were prefiltered ($10\ Hz$ to $1\ kHz$) and digitized at the sampling rate of $2\ kHz$.

The abnormal cases in the data set include chondromalacia of different grades at the patella, meniscal tear, tibial chondromalacia, and anterior cruciate ligament injuries, as confirmed during arthroscopic examination. Due to the inadequacy of the data available for classification of the signals into various types or stages of pathology, studies using this data set have been limited to screening, that is, classification of the signals and the corresponding knee joints as normal or abnormal.

Figure 5.21 shows examples of normal and abnormal VAG signals. Each signal was normalized to the amplitude range $[0, 1]$. The abnormal signal exhibits a higher degree of overall variation, activity, or complexity than the normal signal.

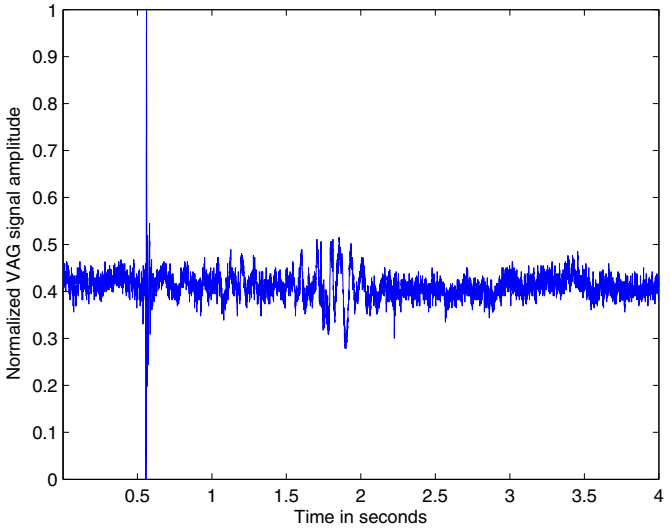


(a)

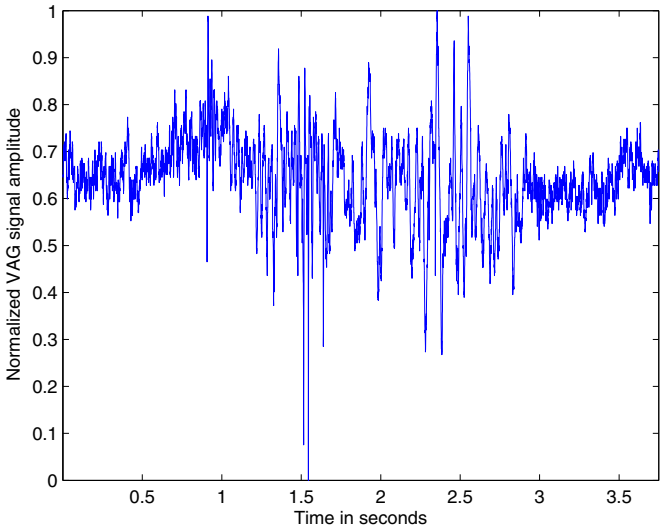


(b)

**Figure 5.21** VAG signal of (a) a normal subject and (b) a subject with knee-joint pathology. Reproduced from R.M. Rangayyan and Y.F. Wu, Screening of knee-joint vibroarthrographic signals using probability density functions estimated with Parzen windows, *Biomedical Signal Processing & Control*, January 2010, 5(1):53–58, with permission from Elsevier. ©Elsevier.

### 5.12.2 Estimation of the PDFs of VAG signals

In the work of Rangayyan and Wu [266], models of the PDFs of VAG signals were derived using the Parzen-window approach [267, 268] to represent their basic statistical characteristics. A histogram was computed by combining all of the normal signals into one group. The histogram, denoted by $h_n(x_l)$, with $x_l$, $l = 0, 1, 2, \ldots, L-1$, represents the $L$ bins used to quantize the range of the values of the signal $x$. Rangayyan and Wu used $L = 100$ bins to represent the normalized range of $[0, 1]$ for the VAG signal values. A large value for $L$ could result in several bins with negligible or zero counts, whereas a small value could cause diminished differences between the histograms for normal and abnormal signals. The value of $L = 100$ was selected based on an analysis of the results with several values of $L$. Similarly, a histogram $h_a(x_l)$ was obtained by pooling together all of the abnormal signals. Each histogram was normalized by dividing by the total number of samples in the population to have unit area under the normalized histogram. A Gaussian fit was then obtained for each of the two histograms, denoted as $g_n(x_l)$ and $g_a(x_l)$.

The Parzen-window approach to obtain a nonparametric estimate of the PDF from a collection of samples was applied as follows [267, 268]. Consider the situation where we have a set of independent samples, $Z = \{z_1, z_2, \ldots, z_K\}$, with an unknown underlying PDF $p(z)$. A nonparametric estimate of $p(z)$ from $Z$ is provided by the function [267, 268]

$$\hat{p}(z) = \frac{1}{K} \sum_{k=1}^{K} \kappa(z - z_k), \tag{5.29}$$

where $\kappa$ is a window or kernel function that integrates to unity. Rangayyan and Wu [266] used

$$\kappa(z - z_k) = \frac{1}{\sigma_P \sqrt{2\pi}} \exp\left[ -\frac{(z - z_k)^2}{2\,\sigma_P^2} \right]. \tag{5.30}$$

The Parzen-window PDF was estimated using the quantized values of the signals, $x_l$, $l = 0, 1, 2, \ldots, L-1$, with $L = 100$ levels, in the normalized range $[0, 1]$. Experiments were conducted with the value of the parameter $\sigma_P$ in Equation 5.30 varying over the range $[0.01, 0.1]$ in steps of $0.01$; the final value was set equal to $0.04$.

Figure 5.22 shows the Parzen-window estimates of the PDFs of the normal and abnormal VAG signals shown in Figure 5.21. Figure 5.23 shows the Parzen-window estimates of the PDFs of the $51$ normal and $38$ abnormal VAG signals in the data set used. The amplitude of the VAG signals has been normalized to the range $[0, 1]$. The figures also show the normalized histogram and the Gaussian fit for each case.

The following observations were made from the PDFs of the normal and abnormal VAG signals:

- In general, the Parzen-window PDFs are closer to the normalized histograms of the VAG signals than the corresponding Gaussian models. The closeness of the fit depends upon the value of $\sigma_P$ used: The smaller the value of $\sigma_P$, the better

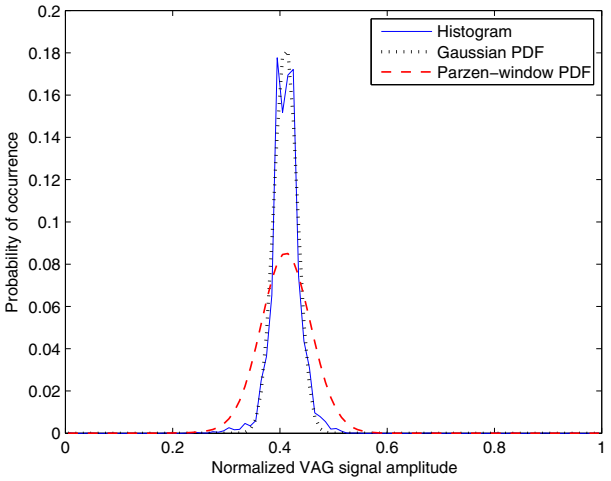


(a)

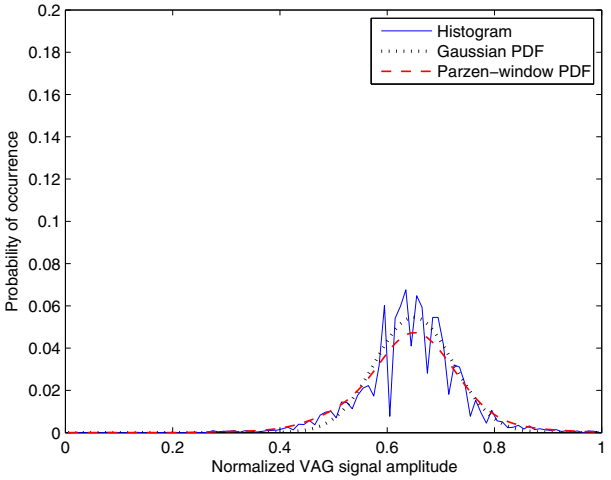


(b)

**Figure 5.22** Nonparametric Parzen-window estimates of the PDFs of the VAG signals in Figure 5.21: (a) of a normal subject and (b) of a patient with knee-joint pathology. The amplitude has been normalized to the range $[0, 1]$. The figure also shows the normalized histogram and the Gaussian fit for each case. The parameters of the Gaussian fit are (a) mean $= 0.4107$, $SD = 0.0216$; and (b) mean $= 0.6499$, $SD = 0.0730$. Reproduced from R.M. Rangayyan and Y.F. Wu, Screening of knee-joint vibroarthrographic signals using probability density functions estimated with Parzen windows, *Biomedical Signal Processing & Control*, January 2010, 5(1):53–58, with permission from Elsevier. 

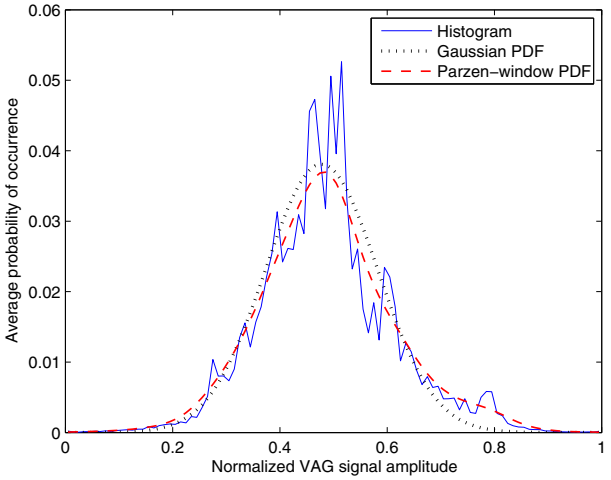


(a)

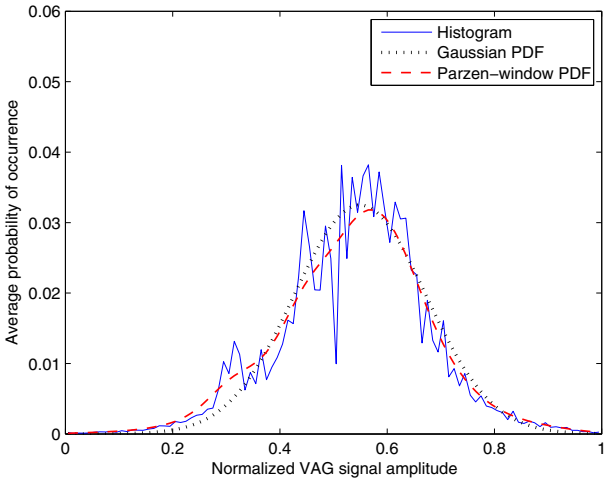


(b)

**Figure 5.23** Nonparametric Parzen-window estimates of the PDFs of VAG signals: (a) derived from VAG signals of 51 normal volunteers and (b) derived from VAG signals of 38 subjects with knee-joint pathology. The amplitude has been normalized to the range $[0, 1]$. The figure also shows the normalized histogram and the Gaussian fit for each case. The parameters of the Gaussian fit are (a) mean $= 0.4778$, $SD = 0.1047$; and (b) mean $= 0.5495$, $SD = 0.1227$. Reproduced from R.M. Rangayyan and Y.F. Wu, Screening of knee-joint vibroarthrographic signals using probability density functions estimated with Parzen windows, *Biomedical Signal Processing & Control*, January 2010, 5(1):53–58, with permission from Elsevier. 

the fit. However, a larger value of $\sigma_P$ is desirable to obtain smooth model PDFs that do not include irrelevant details of the histograms of the signals. A balance needs to be achieved between these two requirements.

- The PDF models for the abnormal signals indicate that the abnormal signals have higher probabilities of occurrence of higher values within the normalized range $[0, 1]$.
- Based on the differences between the PDF models for the normal and abnormal signals, it should be possible to classify VAG signals using parameters derived from their PDFs.
- The apparent differences between the PDF models suggest the existence of different underlying signal-generation processes or statistical models for normal and abnormal VAG signals.

The following section provides details on the derivation of parameters from PDFs for classification of VAG signals.

### 5.12.3 Screening of VAG signals using statistical parameters

VAG signals related to various types of knee-joint pathology have been observed to possess a larger extent of variability over the duration of a swing cycle of the leg than normal VAG signals [94, 95, 264–266, 269–271]. To characterize this nature of VAG signals, Moussavi et al. [94] used the variance of the means of the segments of a given VAG signal; the signals were segmented adaptively using the RLS algorithm. Rangayyan and Wu explored the use of several statistical parameters [272], including $FF$ (see Section 5.6.4), skewness, kurtosis, and entropy [264] as well as an adaptive turns count and the variance of the $MS$ value [265] (see Section 3.2.1) for screening of VAG signals. Other methods that have been proposed for the analysis of VAG signals include AR modeling [95, 96], cepstral coefficients [96], time-frequency distributions (TFDs) [273], and wavelet packet decomposition [270]; see Wu et al. [271] for a review.

As described in Section 3.2.1, various statistical measures may be computed based upon the moments of the PDF of a given signal, $p_x(x_l)$, with $x_l$, $l = 0, 1, 2, \ldots, L-1$, representing the $L$ bins used to span the range of the values of the signal $x$. The $k^{\text{th}}$ central moment of the PDF $p_x(x_l)$ is defined as

$$m_k = \sum_{l=0}^{L-1} (x_l - \mu)^k \, p_x(x_l), \tag{5.31}$$

where $\mu$ is the mean value, given by

$$\mu = \sum_{l=0}^{L-1} x_l \, p_x(x_l). \tag{5.32}$$

See Section 3.2.1 for the definition of several related statistical parameters.

The Kullback–Leibler distance or divergence ($KLD$) between two PDFs $p_1(x_l)$ and $p_2(x_l)$ is defined as [267]

$$KLD(p_1, p_2) = \sum_{l=0}^{L-1} p_2(x_l) \ \ln \left[ \frac{p_2(x_l)}{p_1(x_l)} \right]. \tag{5.33}$$

Rangayyan and Wu [266] computed the $KLD$ between the PDF estimated for the signal to be classified and the PDF models for the normal and abnormal VAG signals. In obtaining the PDF models for the normal and abnormal signals with the limited data set available, the leave-one-out (LOO) method was used: the signal to be classified was left out of the procedure to obtain the Parzen-window model for the corresponding class. In this manner, the signal being tested does not contribute to the training process.

Using only the $KLD$ feature obtained with the Parzen-window models, a normal-versus-abnormal classification accuracy of $73\%$ was obtained with the data set of $89$ VAG signals used. The sensitivity and specificity of classification (screening) were calculated to be $68.42\%$ and $76.47\%$, respectively. The use of $KLD$ with the Gaussian models resulted in poorer performance, with overall accuracy of $69.7\%$. Note that the Gaussian model does not facilitate the characterization of asymmetric or skewed PDFs.

Pattern classification using the set of parameters $(KLD, K, H, \mu, \sigma)$ led to an overall accuracy of $77.5\%$, sensitivity of $71.1\%$, and specificity of $82.4\%$ using radial basis functions (RBF) with LOO. Other combinations of the parameters gave poorer results. Mu et al. [274] obtained better classification performance using some of the features described above but with advanced methods including a genetic algorithm for feature selection and the strict two-surface proximal classifier.

Given the nonstationary nature of VAG signals, it would be advantageous to compute some of the parameters described above using segments of VAG signals instead of their full duration [264, 265]. See Sections 6.6, 8.14, 9.4.2, 9.8.1, and 9.12 for descriptions of other methods for the analysis of VAG signals.

## 5.13 Application: Fractal Analysis of the EMG in Relation to Force

**Problem:** *Fractals exhibit patterns of various levels of complexity. Can fractal analysis be applied to characterize the variations in an EMG signal with respect to the force exerted by a muscle?*

**Solution:** Several biomedical systems and signals exhibit varying levels of complexity in their characteristics and patterns that vary across different states of health and disease. The fractal dimension ($FD$) can be used to represent such complexity in a quantitative manner. Various methods are available to derive estimates of $FD$ from a given signal, as described in the following sections.

### 5.13.1 Fractals in nature

The term "fractal" was coined by Mandelbrot [275] to represent patterns that possess self-similarity at several scales or levels of magnification [276–283]. Fractal geometry has received considerable attention as a mathematical tool to model randomness in nature. Self-similarity refers to the property of an object that has a substructure that resembles its superstructure: Under several levels of magnification, a fractal appears to have the same form. A common example of a self-similar fractal in nature is a fern that has the same pattern repeated at multiple scales in its leaves; broccoli and cauliflower also exhibit fractal patterns. On the other hand, a Euclidean form, such as a square or a triangle, does not retain its original form when magnified. The Cantor bar, the Koch curve, the Sierpinski triangle, and the Hilbert curve are well-known fractals [276, 282].

A fractal is typically formed using a recursive procedure, whereas a Euclidean shape is defined by an algebraic formula. Fractals possess irregular and complex forms that cannot be described adequately using simple Euclidean geometry or shapes. It is readily understood that the dimension of a straight line is unity, that of a square is two, and that of a cube is three. However, a VAG signal that is a 1D function of time, but occupies the 2D space in a more complicated manner than a straight line, may be considered to possess a fractional dimension that is between unity and two. Fractal analysis could be used to model and analyze apparently complex or complicated patterns. However, natural objects may not possess self-similarity at all scales. A real-life pattern does not possess infinite levels of detail or granularity. Furthermore, a natural pattern, when magnified, may appear similar but not exactly identical to its original unmagnified form. This characteristic is referred to as statistical self-similarity. A natural fractal-like object may be viewed as an approximate fractal with statistical self-similarity over a finite range of scales. Fractal analysis is a part of a new set of advanced techniques for nonlinear and dynamic analysis of biomedical signals [284–286].

### 5.13.2 Fractal dimension

Consider a self-similar pattern that exhibits a number of self-similar parts represented by the variable $a$, at the reduction factor of $1/s$. The reduction factor is related to the measurement scale. The self-similarity dimension ($D$) is defined in a power-law relationship as [276]

$$a = \frac{1}{s^D}\,. \tag{5.34}$$

Applying the log and solving for $D$, we get

$$D = \frac{\log(a)}{\log(1/s)}\,. \tag{5.35}$$

The slope of a plot of the log of the number of self-similar parts, $\log(a)$, versus the log of the reduction factor, $\log(1/s)$, can provide an estimate of $D$. A straight-line

approximation could be fitted to estimate the slope. Two popular methods to estimate $FD$ are the ruler method and the box-counting method [276], which are described in the following paragraphs.

**The ruler method:** Using rulers of different length, the total length of a pattern or signal can be estimated to different levels of accuracy. If a large ruler is used, the small details in the given pattern are ignored. As smaller and smaller rulers are used, finer details get measured. The measured or estimated length increases and improves in accuracy as the size of the ruler decreases. An estimate of $FD$ is obtained from the slope of a straight-line fit to a plot of the log of the measured length versus the log of the measuring unit or ruler size.

Let $u$ be the length measured with a ruler of size $s$. The precision of measurement is represented by $1/s$. A fractal is expected to satisfy the power law [276]

$$u = c\,\frac{1}{s^d}\,, \tag{5.36}$$

where $c$ is a constant of proportionality and $FD = 1 + d$. Applying the log, we have

$$\log(u) = \log(c) + d\,\log(1/s)\,. \tag{5.37}$$

The slope of a plot of $\log(u)$ versus $\log(1/s)$ provides an estimate of $FD$ as $FD = 1 + d$.

If we let $u = ns$, where $n$ is the number of times the ruler is used to measure the length $u$ with the ruler of size $s$, then

$$\log(n) = \log(c) + (1 + d)\,\log(1/s)\,. \tag{5.38}$$

The slope of a plot of $\log(n)$ versus $\log(1/s)$ directly provides an estimate of $FD$.

**The box-counting method:** The box-counting method [276, 282, 287–290] involves partitioning the pattern or signal space into square boxes of equal size, and counting the number of boxes that contain a part of the signal. The process is repeated by partitioning the signal space into smaller and smaller squares. The log of the number of boxes counted is plotted against the log of the magnification index for each stage of partitioning. The slope of the straight line fitted to the plot gives an estimate of the $FD$.

**Higuchi's method:** Higuchi [291] proposed an algorithm to estimate the $FD$ of a signal by computing measures of the length of the signal using multiple versions of the signal reconstructed for varying measurement intervals. Given a signal $x(n)$, $n = 1, 2, \ldots, N$, the method creates new signals as [291, 292]

$$x_k(m) = x(m), x(m+k), x(m+2k), \ldots, x\left(m + \lfloor\frac{N-m}{k}\rfloor\, k\right), \tag{5.39}$$

for various values of $k$, where $k$ and $m$ are integers with $m = 1, 2, \ldots, k$. Here, $m$ represents the initial point and $k$ is the interval between the points of $x_k(m)$. The length of each derived signal is computed as

$$L(m,k) = \frac{1}{k}\,\frac{N-1}{k\left\lfloor \frac{N-m}{k} \right\rfloor} \sum_{i=1}^{\left\lfloor \frac{N-m}{k} \right\rfloor} |x(m+ik) - x[m+(i-1)k]| \tag{5.40}$$

and

$$L(k) = \frac{1}{k} \sum_{m=1}^{k} L(m,k). \tag{5.41}$$

The slope of a straight-line fit to a log–log plot of $L(k)$ against $1/k$ gives the $FD$ of the original signal.

When applying the ruler or box-counting methods to a signal or pattern, it is important to select an appropriate range of the size of the ruler or the box [276, 282, 289]. The range of size needs to be related to the range of the values of the signal for both the independent variable (such as time) and the dependent variable (such as voltage). It could be convenient to normalize both ranges of a given signal to $[0, 1]$ and to define the ruler or box size in relation to the normalized variables.

For discussions on other methods of fractal analysis, see Section 6.6, Cabral and Rangayyan [282], and Banik et al. [293].

### 5.13.3 Fractal analysis of physiological signals

Fractal properties have been observed in several physiological structures and processes. Many anatomical structures have fractal-like appearance, such as the coronary arteries, venous branching patterns, bronchial trees, certain muscle fiber bundles, and the His–Purkinje network in the ventricles [294]. The branching pattern of the His–Purkinje network of conduction pathways provides an efficient way to distribute the depolarization stimulus to the ventricles. The electrogenesis of the QRS complex in the ECG has been modeled by using a fractal-like conduction system. The normal QRS complex has been shown to follow an inverse-power-law distribution of frequency content in the log–log scale [295]; this property has been noted as being consistent with depolarization of the myocardium by a self-similar branching network [294]. Studies of such branching networks used to depolarize a network of cells via computer modeling have shown that, after 10 generations of branching, it is possible to simulate realistic QRS complexes [296]. The frequency content of QRS complexes has been shown to be affected by changes in the geometry of the branching network.

Goldberger et al. [295] and Goldberger and West [297] showed that the rhythm of a healthy heart is not highly regular, but that it is a temporal fractal with a high degree of variability in the heart rate. The PSD of a time-series representation of the heart rate follows the inverse power law (see Section 6.6 for related discussion). It has been shown that, in the case of time series of heart rate, the loss of physiological complexity can lead to greater regularity. The phenomena associated with fractals,

self-similar scaling, $1/f$ noise, and inverse-power-law distributions offer interesting models as well as useful methods to characterize physiological processes and biomedical signals [297].

Li et al. [298] applied a method of fractal and wavelet-based spectral analysis to analyze EEG signals of rats. It was hypothesized that variations in $FD$-related parameters, such as the Hurst and spectral exponents, can be used to describe the dynamic characteristics of the brain in different states, in particular before seizures. They found that the method revealed characteristic signs of an approaching seizure, including the emergence of long-range correlation and decrease in the $FD$ value. Liang et al. [299] applied the Hurst exponent, extracted from EEG recordings, as a measure of the effects of anesthesia on brain activity. The maximal overlap discrete wavelet transform (DWT) was used to suppress the effects of artifacts in the EEG and the scaling properties of the data in designated frequency bands were calculated prior to estimation of the Hurst exponent. It was observed that the Hurst exponent decreased (especially in low-frequency bands) when anesthesia deepened and that it is a useful measure for estimating the depth of anesthesia.

Shah et al. [300] studied acceleration signals obtained from finger joints of patients with calcium pyrophosphate deposition disease, rheumatoid arthritis, or spondyloarthropathy of the finger joint. The ruler method was used to estimate $FD$. The results showed that there were significant differences between the $FD$ values of acceleration signals from patients in the three categories. Specifically, the $FD$ values of acceleration signals from the patients with calcium pyrophosphate deposition disease ($1.709 \pm 0.097$) were higher than those of patients with rheumatoid arthritis ($1.6 \pm 0.069$) or spondyloarthropathy ($1.569 \pm 0.081$).

There is increasing interest in nonlinear dynamical analysis of biomedical signals using several recently developed methods related to fractals, chaos, and nonlinear modeling [282, 284–286]; see Stam [301] for a detailed review of nonlinear dynamical analysis of the EEG and other signals. The recently developed methods of nonlinear dynamical analysis are expected to make it possible to study self-organization, pattern formation, and attractors of trajectories in the state space of nonlinear and complex systems that may not be captured by traditional linear methods.

For discussions on the application of fractal analysis to images of breast lesions in mammograms, see Rangayyan and Nguyen [302], Cabral and Rangayyan [282], and Banik et al. [293].

### 5.13.4 Fractal analysis of EMG signals

We have seen several examples of the increasing complexity of EMG signals with increasing force and studied many methods to capture such complexity in quantitative terms; see, for example, Figure 1.20 and Sections 5.9, 5.10, and 5.11. Figure 5.24 shows the variation of $FD$, obtained using Higuchi's method, for the EMG signal shown in Figure 1.20. The EMG signal was first filtered with a Butterworth lowpass filter of $6^{\text{th}}$ order and cutoff frequency of $300\ Hz$. Segments of duration $1\ s$ were cut for each level of contraction to estimate $FD$. It is evident that $FD$ increases with the level of contraction (except for the last level of contraction) with high correlation.

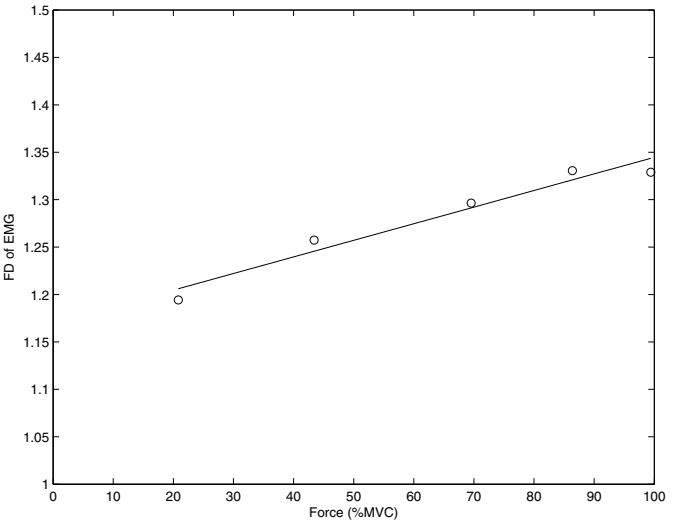


**Figure 5.24** Variation of $FD$ with the level of muscle contraction for the EMG signal shown in Figure 1.20; $r^2 = 0.95$. Figure courtesy of Faraz Oloumi.

Anmuth et al. [303] applied fractal analysis to surface EMG signals obtained from the FDI at various levels of isometric contraction. A correlation coefficient of $0.991$ was obtained between pooled $FD$ and %MVC data for $10$ subjects.

Gitter and Czerniecki [304] studied the use of $FD$, estimated using the box-counting method, in the analysis of EMG signals. They obtained needle EMG signals at various levels of contraction of the biceps brachii muscle. $FD$ values, averaged over three repetitions of each level of contraction, were obtained in the range $[1.1, 1.4]$ and exhibited positive correlation with force. However, whereas the correlation was high with $r = 0.94$ in the range $[10, 70]$ %MVC, it was low with $r = 0.35$ in the range $[70, 90]$ %MVC.

Gupta et al. [305] studied the variation of the $FD$ of surface EMG signals of the biceps brachii during flexion and extension of the arm at various speeds and with different loads placed on the palm. Using linear regression, they found $FD$ to be correlated well to both the load ($r = 0.99$) and the rate of flexion-extension ($r = 0.98$).

Muscle fatigue is known to cause reductions in the mean and median frequency of the related EMG signals. Ravier et al. [306] applied the $1/f$ model (see Section 6.6.1) to analyze EMG signals related to muscle force and fatigue. They found that the right slope of the EMG spectrum (beyond the peak frequency in the range of $60 - 90\ Hz$) decreased with increasing levels of force, but there was no substantial effect of fatigue on the slope. However, Talebinejad et al. [307] applied multifractal detrended fluctuation analysis methods to obtain optimal Hurst exponents, which showed a high degree of correlation with the progress of fatigue; see also Talebinejad et al. [308, 309].

## 5.14 Remarks

We have now reached the stage in our study where we can derive parameters from segments of biomedical signals. In the present chapter, we focused our attention on characteristics that could be observed or derived in the time domain. The parameters considered were designed with the aim of discriminating between different types of waveshapes, or of representing change in waveform complexity through the course of a physiological or pathological process. We have seen how the various parameters explored in the present chapter can help in distinguishing between normal and ectopic ECG beats, and how certain measures can serve as quantities that are correlated with levels of physiological activity, such as respiration and muscular contraction.

It should be borne in mind that, in most practical applications, a single parameter or a couple of measures may not adequately serve the purposes of signal analysis or diagnostic decision making. A single parameter such as $FF$ or $SL$ may assist in distinguishing some types of PVCs from normal ECG beats; however, several cardiovascular diseases and defects may cause changes in the ECG signal that may lead to similar variations in the $FF$ or $SL$ values. A practical application would need to maintain a broad scope of analysis and use several parameters to detect various possible abnormalities. As always, an investigator should consider the possibility that a parameter observed to be useful in, for example, ECG analysis in the time domain, may serve the needs in the analysis of some other signal, such as the PCG or EMG, in a different domain.

## 5.15 Study Questions and Problems

1. Prove that the values of $FF$ of a sinusoidal wave is equal to unity.

2. The following discrete-time signals are defined over the interval 0 to 10 $s$ with the sampling frequency being 1 $Hz$: (a) $x_1(n) = u(n) - u(n-5)$. (b) $x_2(n) = 2u(n-3) - 2u(n-8)$. (c) $x_3(n) = u(n-2) - u(n-9)$. (d) $x_4(n) = u(n-2) - u(n-10)$. $u(n)$ is the discrete-time unit step function. The $SL$ of a signal $x(n)$ is defined as

$$SL = \frac{\sum_{n=0}^{N-1} w(n)\, x^2(n)}{\sum_{n=0}^{N-1} x^2(n)},$$

   where $w(n)$ is a nondecreasing weighting function, and $N$ is the number of samples in the signal. Let $w(n) = n$, $n = 0, 1, 2, \ldots, N-1$. Draw sketches of each signal with the weighting function $w(n)$ superimposed. Compute the $SL$ values for the four signals given. Interpret your results and compare the characteristics of the four signals in terms of their $SL$ values.

3. You are given a signal with the samples $\{0, 0, 2, 2, 3, -3, 2, 0, 0\}$ and a template with the samples $\{1, -1\}$. Perform the template matching operation and derive the sample values for the output. Provide an interpretation of the result.

4. Discuss the similarities and differences between the problems of (i) detection of spike transients in EEG signals, and (ii) the detection of QRS complexes in ECG signals.

5. You have been hired to develop a heart-rate monitor for use in a coronary-care unit. Design a system to accept a patient's ECG signal, filter it to remove artifacts and noise, sample the signal, measure the heart rate, and set off alarms as appropriate. Provide a block diagram of the system, with details of the signal processing steps to be performed in each block. Specify the important parameters for each processing step.
6. A needle EMG signal under low levels of muscle contraction was observed to contain a mixture of three trains of MUAPs. One of the trains contains quasiperiodic occurrences of a monophasic MUAP, the second contains occurrences of a biphasic MUAP, and the third contains occurrences of a triphasic MUAP. It was also observed that the MUAPs do not overlap in the EMG signal. Propose a signal analysis procedure to: (a) detect the occurrence (location in time) of each MUAP of each type individually and (b) determine the firing rate of each motor unit. Note that each MUAP needs to be detected and labeled as being one of monophasic, biphasic, or triphasic type.

   Your solution should include: (i) plots of the EMG signal (make up one according to the description above) with labels for the components; (ii) plots of the signal at various stages of your procedure; (iii) equations for important steps of your signal analysis procedure; and (iv) statements describing the reason or logic behind each step you propose.
7. A researcher is attempting to develop a digital signal processing system for the acquisition and analysis of heart sound signals (PCG signals). Assist the researcher in addressing the following concerns and problems: (a) What are the typical bandwidths of normal PCG signals and those with murmurs? What is the recommended sampling frequency? (b) What are the sources of artifacts that one has to consider in recording PCG signals? Name one physiological source and one other source, and recommend techniques to limit or eliminate both. (c) How can one identify the locations of S1 and S2? Which other biomedical signals would you recommend for assistance in this problem? Draw schematic diagrams of the signals and identify the corresponding cardiac events and timing relationships. (d) Propose a technique to obtain the envelope of the PCG signal. List all steps of the method you propose and provide the required parameters. (e) Draw schematic PCG signals and their envelopes over one cardiac cycle for a normal case, a case with systolic murmur, and a case with diastolic murmur. Identify each event in each case.
8. You are given a database of SMUAPs containing several types of normal and abnormal patterns. Each signal record has one SMUAP. The patterns and features of interest are: (i) Monophasic SMUAPs. (ii) Biphasic SMUAPs. (iii) Triphasic SMUAPs. (iv) Polyphasic SMUAPs with more than three phases.

   (a) Propose two parameters (computed features) to help in separating the four classes of SMUAPs. Give the required equations or procedures and explain their relationship to the signal characteristics described above. Describe conditions or preprocessing steps that are required in order for your methods to work well. (b) Draw a schematic plot of the feature-vector space and demarcate regions where you expect features of the four SMUAP types to lie. (c) State decision rules to classify the four SMUAP types using the two measures you propose.
9. Why is the ST segment of the ECG relevant in diagnosis? Recommend signal analysis techniques for the analysis of ST segment variations in clinical applications.
10. A researcher new to the field of biomedical signal analysis is assigned a project on the analysis of heart sounds and murmurs. The researcher is provided with a database of PCG signals of four types: (a) normal, (b) systolic murmur, (c) diastolic murmur, and (d) systolic and diastolic murmur.

The researcher surfs the internet and obtains two programs to compute the $ZCR$ using a moving window of 20 $ms$ and a filtered envelope of a given signal. The sampling rate used is $1,000$ $Hz$. Although the programs generated graphs of the given signal, the $ZCR$, and the smoothed envelope, the researcher encountered difficulties in interpreting the results.

Assist the researcher by providing the following information: (i) For each type of PCG signal listed above, draw plots of a typical PCG signal, its $ZCR$ as a function of time, and the averaged envelope. Explain the important expected characteristics of the results. (ii) Estimate the ranges of $ZCR$ values (using a moving window of 20 $ms$) for typical normal heart sounds and murmurs. Explain your procedure and assumptions.

11. A researcher has obtained a system to record the EMG signal from a muscle that is directly involved in breathing (respiration). Help the researcher in understanding the nature of the signal and developing a signal processing system to analyze the signal as follows: (a) Draw a schematic representation of the EMG over two cycles of respiration, showing the ranges of inspiration and expiration. (b) Propose an algorithm to obtain the envelope of the EMG signal. Describe the nature and purpose of each step in your algorithm. Give an equation for each step, and plot the result of the operation on the EMG signal. (c) Propose a method to obtain a measure of activity (to indicate how 'busy' the signal is) as a function of time, in order to characterize the variation in the signal with breathing. Give an equation and describe the nature of the method. Plot the result of the operation on the EMG signal. (d) The peak values in the envelope and activity functions over a given cycle of respiration are expected to be correlated with the peak air flow to the lungs. Propose algorithms to detect the peak envelope and peak activity values. (e) For each procedure that you propose in items (b), (c), and (d) above, discuss potential artifacts that could mislead your procedure and indicate how you would prevent them.

12. A researcher is developing methods to extract features from ECG signals to distinguish between normal beats and PVCs. Draw typical waveforms of the two types of beats and explain the major differences between them in qualitative terms. Propose two quantitative measures or features to characterize the differences between normal beats and PVCs. Give an equation or a step-by-step algorithm to compute each feature.

13. A student new to the field of biomedical engineering approaches you seeking assistance to develop methods to analyze the relationship between the force produced by contracting a muscle and the corresponding EMG signal. Help the student by providing detailed responses to the following questions and requests:

    (a) How can one acquire EMG signals corresponding to different levels of force? (i) How many electrodes are required? (ii) Where and how should the electrodes be placed? (iii) How can one get another signal or variable that is directly proportional to the force? (iv) What should be the settings for the bandwidth of the filters for the EMG signal? (v) What should be the settings for the bandwidth of the filters for the force signal? (vi) What should be the sampling frequency? (vii) Give a step-by-step experimental procedure to acquire the required signals. (viii) Draw a schematic diagram to illustrate the expected nature of the EMG and force signals.

    (b) (i) What are the precautions to be taken in recording the signals? (ii) List one potential source each for random noise, structured noise, and physiological artifact that could corrupt the EMG signal. (iii) For each source of noise or artifact that you identify, recommend a procedure to prevent the same. (iv) For each source of noise or artifact that you identify, recommend a postacquisition procedure to remove the same.

(c) (i) What kind of measures or parameters may one derive from an EMG signal so that the measures vary in proportion to muscular force? (ii) Give equations to define three parameters that are suitable for this purpose. For each parameter, give a step-by-step procedure to compute the parameter from the EMG signal. (iii) Explain the expected relationships between the three parameters that you recommend and muscular force. Draw a plot with the force on the abscissa ($x$-axis) and the proposed parameters on the ordinate ($y$-axis).

14. Given a sampled signal, $x(n)$, $n = 0, 1, 2, \ldots, N-1$, write an equation to compute the *variance*, $\sigma_x^2$, of the signal. Give the definitions of the parameters *mobility* and *form factor*. Explain how the three parameters mentioned above may be computed and used to analyze the relationship between the force generated by muscular contraction and the related EMG signal.

15. Explain the concept of an envelope of a signal. Give a step-by-step algorithm to compute an envelope of a signal. Include at least two equations for parts of the procedure. Draw a normal PCG signal over one cardiac signal and a corresponding envelope. Explain the relationships between the two and suggest a use of the envelope in a practical application.

## 5.16 Laboratory Exercises and Projects

*Note:* Data files related to the exercises are available at the site

`http://people.ucalgary.ca/~ranga/enel563`

1. The signal in the file emg_dog2.dat was recorded from the crural diaphragm of a dog using fine-wire electrodes sewn in-line with the muscle fibers and placed 10 $mm$ apart. The signal represents two cycles of breathing, and has been sampled at 10 $kHz$. (See also the file emg_dog2.m.)

   Write a MATLAB® program to perform full-wave rectification (absolute value) or half-wave rectification (threshold at zero, with the mean value of the signal being zero). Apply a lowpass Butterworth filter of order four and cutoff frequency in the range 5 to 20 $Hz$ to the result. Analyze and evaluate the results with the two methods of rectification and at least two different lowpass cutoff frequencies. Compare the results with the envelope provided in the file emg_dog2_env.dat.

2. The $RMS$ value of a signal within a specific duration is related to the average power level of the signal. Write a MATLAB® program to compute the $RMS$ value at each instant for the EMG signal in the file emg_dog2.dat by using a causal short-time analysis window of duration in the range $50 - 150$ $ms$. Use at least two different window durations and analyze the results. (See also the file emg_dog2.m.)

3. Develop a program to compute the turns count in causal moving windows of duration in the range $50 - 150$ $ms$. Apply the method to the EMG signal in the file emg_dog2.dat. (See also the file emg_dog2.m.) Study the results for different thresholds in the range $0 - 200$ $\mu V$. Compare the envelope, $RMS$, and turns count curves in terms of their usefulness as representatives of inspiratory airflow (data provided in the file emg_dog2_flo.dat).

4. The file safety.wav contains the speech signal for the word "safety" uttered by a male speaker, sampled at 8 $kHz$. (See also the file safety.m.) The signal has a significant

amount of background noise (as it was recorded in a computer laboratory). Develop procedures to derive short-time $RMS$, turns count, and ZCR in moving windows of duration in the range $10 - 100\ ms$. Study the variations in the parameters in relation to the voiced, unvoiced, and silence (background noise) portions of the signal.

What do you expect the results to be if the procedures are applied to the first derivative of the signal? Confirm your assertions or expectations by performing the study.

5. Develop a program to derive the envelogram. Apply the procedure to the PCG signals in the files pec1.dat, pec33.dat, and pec52.dat. (See the file plotpec.m.)

   Extend the procedure to average the envelograms over several cardiac cycles using the ECG as the trigger. How will you handle the variations in the duration (number of samples) of the signals from one beat to another?

6. The ECG signal in the file ecgpvc.dat contains a large number of PVCs, including episodes of bigeminy. (See the file ecgpvc.m.) Apply the Pan–Tompkins procedure to detect and segment each beat. Label each beat as normal or PVC by visual inspection. Record the number of beats missed, if any, by your detection procedure.

   Compute the $RR$ interval and the form factor $FF$ for each beat. Use a duration of 80 samples ($400\ ms$) spanning the QRS–T portion of each beat to compute $FF$. The P wave need not be considered in the present exercise.

   Compute the mean and $SD$ of the $FF$ and $RR$ values for the normal beats and the PVCs. Evaluate the variation of the two parameters between the two categories of beats.

7. Obtain EMG signals related to various levels of muscular activity or force. You may use the data files EMGforce.txt and EMGforce2.txt as well as the program EMGforce.m provided; the sampling rate is $2,000\ Hz$ per channel. Normalize the force signal such that the minimum value is zero and the maximum value (corresponding to MVC) is 100. Filter the force signal to remove noise and artifacts. Plot the EMG signal (in $mV$) and normalized force (in %MVC) against the time axis.

   Develop a program for automatic identification of portions (segments) corresponding to each level of contraction within which the force remains close to the corresponding peak values. For each segment of the EMG signal identified as above, compute four suitable parameters. Ensure that your list of EMG features includes the following: $RMS$ value, form factor, and turns count. Compute also the average force (in %MVC) for each segment.

   Plot the values of the various parameters versus force in %MVC. Label the axes with the appropriate units. Analyze the results in terms of statistical variation of the parameters in relation to force. Using the `polyfit` function in MATLAB®, obtain a straight-line (linear) fit to represent the variation of each EMG parameter versus force. Use `polyval` to evaluate the values of the dependent variable given by the model for the available values of the independent variable. Superimpose the linear models (straight-line fits) obtained on the plots of the parameters in the preceding step. Analyze the results.

   Compute the correlation coefficient, $r$, with $r^2$ given by the formula

$$r^2 = \frac{\left[\sum_{n=1}^{n=N} x(n)\,y(n) - N\,\bar{x}\,\bar{y}\right]^2}{\left[\sum_{n=1}^{n=N} x^2(n) - N\,\bar{x}^2\right]\ \left[\sum_{n=1}^{n=N} y^2(n) - N\,\bar{y}^2\right]},$$

   where $N$ is the number of samples of $x$ or $y$ representing each of the EMG parameters or force, and $\bar{x}$ is the mean of $x$. Using $r$, analyze the goodness of fit for each parameter

and discuss the appropriateness of the linear model. Tabulate the parameters of the linear model and $r$ for each of the EMG parameters. Analyze the results and describe your findings. Perform all of the above steps with the two EMG signals mentioned above. Analyze and compare the results.